Utrecht University

Deltares

Master Thesis

Modelling waves and currents in muddy coastal areas, with a focus on the Suriname coastal zone

by

Maria Eirini Tzampazidou

Supervised by:

Prof. Dr. H.E. de Swart
B.P. Smits, MSc.
J. de Vries, MSc.
A. Nnafie, Phd
Prof. Dr. S.M. de Jong

Institute of Marine and Atmospheric Sciences
MSc. Climate Physics
October 2020

Abstract

The mudbanks in front of the coast of Suriname are an important coastal feature and play a key role in coastal evolution by governing the flow and wave characteristics. Suriname is located in the center of the Guiana basin and it is characterized by its erosional muddy coastal area. The Amazon river is supplying the Guiana basin with about $7 - 10 \cdot 10^8$ tons of sediment every year, leading to the formation of long mudbanks that migrate along its coasts. Moreover, the trade winds, which arrive mainly from the northeast, prevent the large Amazon plume as well as the mudbanks to extend further than 30 km offshore. Hydrodynamics in Suriname are also influenced by semi-diurnal tides that acquire a tidal range of up to 2.8 m and by waves that reach up to 4 m offshore during extreme conditions.

Measures need to be taken in order to prevent coastal erosion and flooding and to compensate for the imminent sea level rise. Although field campaigns took place in the past, the effect of the mudbanks on waves and tidal currents has not been extensively studied. A modelling approach is needed in order to understand in detail the complex dynamics that govern this coastal area. This study aims at identifying the correct tools in order to close that knowledge gap and provide a detailed analysis on the hydrodynamics of the area. More particular, SWAN-Mud and Delft3D-FLOW are used for the first time in order to study the dynamics in the coastal area of Suriname.

The state of the art numerical wave model SWAN-Mud is used in order to simulate waves in the muddy coastal area of Suriname. Particular attention is paid to the sensitivity of results to using different formulations for wave energy dissipation by mud. DELFT formulation (Kranenburg, 2011) shows that waves are severely dissipated as soon as they arrive at the mud layer: significant wave height reduces instantly, total and mud-induced dissipation increase sharply, wave energy is shifted towards larger frequencies, waves refract up to 50 degrees towards the coast (southwards) and orbital velocity decreases as a result of wave dissipation. DELFT formulation is in agreement with a previous study by Winterwerp (2007) at the Guyana coastline, but Gade formulation, which is tested as well, is found to have similar results except for the wave energy distribution (Wells and Coleman, 1981).

Furthermore, the commonly-used numerical flow model Delft3D-FLOW is used in order to simulate tidal currents in the coastal area of Suriname. The main tidal characteristics are in accordance with findings in the literature, i.e. M2 is the most dominant tidal component (Augustinus, 1978), tides arrive perpendicular to the coast, and the tidal phase does not vary significantly Kagan and Sofina (2014). A coupling between Delft3D-FLOW and Delft3D-WAVE does not take place, as the latter uses the regular version of SWAN that cannot take into account the mud layer. Results from Delft3D are expected to be of higher accuracy if it is coupled to SWAN-Mud. In this case, it will be possible to model erosion, transport, and deposition of mud.

Acknowledgements

The first thing I would get as a response every time I was telling to someone that I have four supervisors for my thesis was something like: that should be difficult! But throughout these months I was feeling really lucky. I knew that if I had issues with my models I would go to Bob and to Abdel, and if had questions about Suriname then Job would have the answer and if I had problems with the physics then Huib would send me the most complete answer I could find! Of course sometimes it was a bit stressing as well, because instead of a regular weekly meeting with your supervisor, I almost had a weekly presentation in front of a group of experts! But what could train me better than this?

So I would like to thank each one of you. Huib, you acted like a real mentor, always advising wisely on how to proceed and how to overcome every difficulty we faced. Bob, no matter the coronavirus situation, you were always present no matter your strict schedule, to answer every question I had, provide an alternative solution and really support me. Job, I would never be so interested in Suriname, unless I had a supervisor like you! You are really inspiring and always ready to help. Abdel, your experience in modeling saved me a lot of time, and you know how valuable this is! You were always willing to teach me, and I do appreciate it. Steven was also present in our meetings, and although I did not have the chance to meet him in person I recognised a really kind person.

Besides my mentors, I wanted to thank some more people. Han Winterwerp was present since the beginning of my thesis with his popular paper in Guyana, and I finally got the chance to meet him, and receive even more valuable feedback. Thank you very much. Wouter Kranenburg, I would also like to thank you, as you also tried to find a way to help me with this very tricky SWAN-Mud.

Furthermore, I would like to thank my classmate, Raymond. You supported me since the beginning of my masters and especially during this difficult time of the coronavirus situation, you were always present to discuss mud-related issues!

Finally, I do not know how to thank my boyfriend Konstantinos, and my parents Eleutheria and Panagiotis, for always being next to me and especially during the quarantine. Your love and your support is priceless.

Contents

1 Introduction **6**
1.1 Coastal variability around the world . . . 6
1.2 Area description - Suriname coastal zone . . . 6
1.2.1 Hydrodynamic processes . . . 7
1.2.2 Morphology . . . 8
1.2.3 Potential problems in the muddy coastal area of Suriname . . . 9
1.3 Overview of available knowledge and knowledge gaps . . . 10
1.4 Research objective and research questions . . . 11

2 Materials and methods **13**
2.1 Theoretical background . . . 13
2.1.1 SWAN-Mud . . . 13
2.1.2 Delft3D . . . 19
2.2 Model set up . . . 20
2.2.1 Bathymetry . . . 20
2.2.2 Design of the mudbanks . . . 21
2.2.3 SWAN-Mud Model . . . 21
2.2.4 Delft3D Model . . . 22
2.2.5 Design of experiments . . . 23
2.3 Methods to analyse model outputs . . . 24

3 Results **26**
3.1 Experiments with SWAN-Mud . . . 26
3.1.1 Extreme conditions . . . 26
3.1.2 Normal conditions . . . 34
3.2 Experiments with Delft3D . . . 39

4 Discussion **43**
4.1 Model assumptions . . . 43
4.2 Reprodicibility of results of earlier studies . . . 44
4.3 Experiments with SWAN-Mud for the case in Suriname coast . . . 45
4.4 Experiments with Delft3D . . . 45
4.5 Recommendations for further research . . . 46

5 Conclusions **48**
5.1 First research question . . . 48
5.2 Second research question . . . 48

A Appendix **50**
A.1 Reproduction of earlier work 50
A.2 Results on reproduction of earlier work 52
A.2.1 Experiment 1: 1D case Winterwerp 2007. 52
A.2.2 Experiment 2: Effect of the mudbanks on waves - Guyana case. 53
A.2.3 Experiments 3 and 4: Optimum mud layer thickness for maximum wave attenuation. 56
A.2.4 Implications of the results 56

Chapter 1

Introduction

1.1 Coastal variability around the world

According to Davis and Fitzgerald (2005) a coastal zone is defined as any part of land that is affected by marine processes like waves, tides, winds, biota or salinity.

(a) (b)

Figure 1.1: (a): Example of a muddy coast: Stewart island, New Zealand (Britannica, 2007). (b): Example of a sandy coast: gently sloping, depositional beach: San Jose Island, Texas, United States (Morton et al., 2004).

There are two coastal types according to the sediment class which characterizes them. There are muddy coasts, which consist of sediments with particles smaller than 63 µm (Healy, 2005) and sandy coasts, which consist of sand-size coarse sediments 0.063–2 mm (Short, 2005). Figure 1.1a shows a characteristic tidal mudflat in Stewart Island, New Zealand and Figure 1.1b shows a characteristic sandy coast in San Jose island, Texas, United States.

The focus of this report is on muddy coasts, and more specifically on the coast of Suriname.

1.2 Area description - Suriname coastal zone

The Guiana basin is located in the north-eastern part of south America. It stretches 1800 km from the Amazon to the Orinoco river and it is referred to as the Amazon-Orinoco coast (A-O coast) according to Anthony (2013). The source of the large deposits of mud in the area is the Amazon river, which exports approximately $(7 - 10) \cdot 10^8$ tons of sediments every year to this area. Suriname is found in the center of this area, between Guyana and French Guiana (see Figure 1.2).

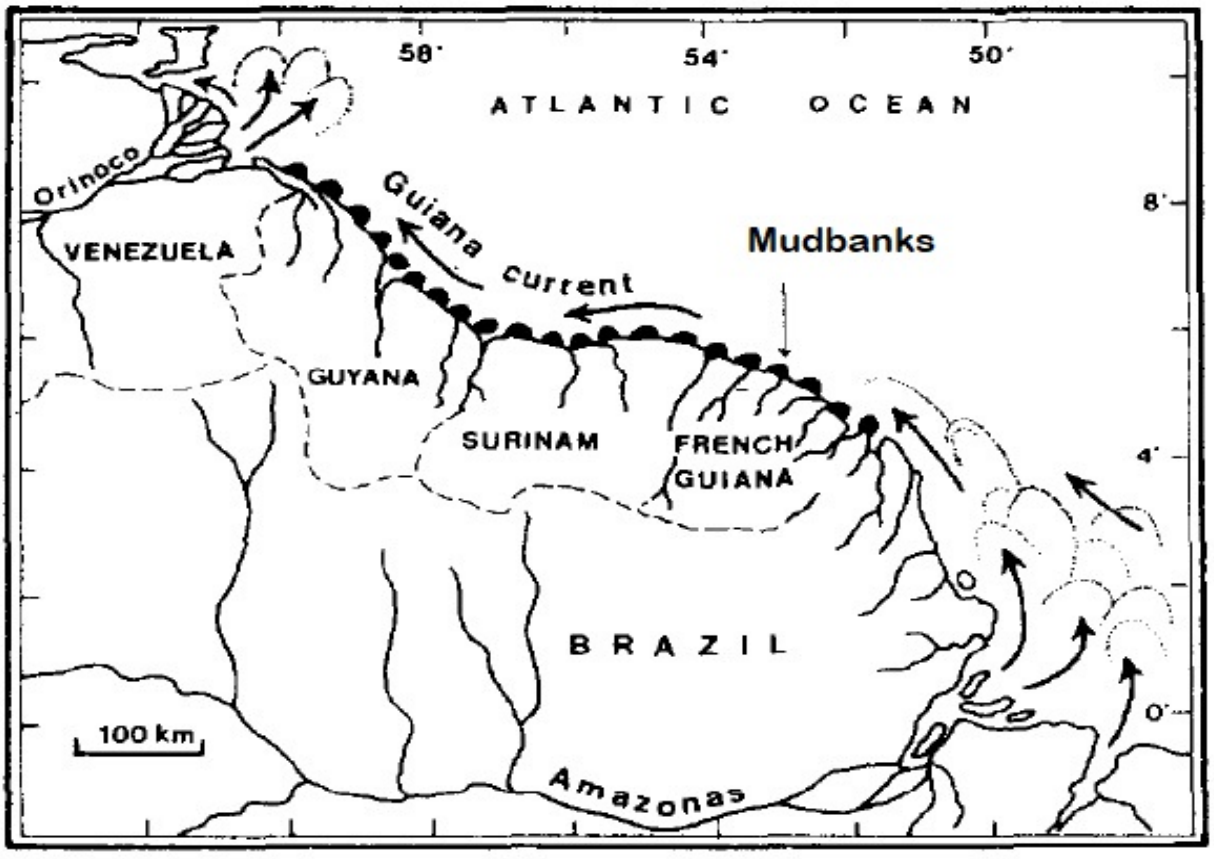

Figure 1.2: Map of South America (Froidefond et al., 1988). The Orinoco river is found in the North-West (NW) corner, while Amazon river is found in the South-East (SE) corner. The area between Orinoco and Amazon river is often referred to as Guiana basin or A-O coastline. Suriname is located in the center. The arrows in the NW, show the river outflow from Orinoco, the arrows in the SE show the river outflow from Amazon and the arrows along the Guiana coast represent the Guiana current. The thick shore-face attached black patches represent the mudbanks observed in the area.

1.2.1 Hydrodynamic processes

Water motion in the area of the coast of Suriname is influenced by the joint action of ocean tides, ocean swell, ocean currents, (local) wind and river outflow (Amazon river and local rivers). The Coriolis effect is negligible since Suriname is located very close to the equator (latitude is about 4°N) (Augustinus, 1978).

The trade winds play a key role in the hydrodynamics of the area, as they force the system with waves and a persistent westward current. The trade winds are from the north-east (NE) and they are mainly active from December to May. Waves arrive at the coast from the same direction: NE. Wind waves that are generated by trade winds usually have wave periods (T_s) of 6-8 s, and wave heights (H_s) of 1-2 m, but in extreme conditions this value approaches 4 m (Augustinus, 2004; Anthony, 2013). The (trade) wind also exerts stresses to the ocean surface. This results in the generation of the westward along-shelf flow of the North Brazil Current (Geyer et al., 2004).

The tide is semi-diurnal, with spring tides up to 2.8 m and neap tides to 1 m. Tidal currents are mainly perpendicular to the coast (Nedeco, 1968). The combined action of the cross-shore tidal currents and the Guyana current generates zig-zag particle trajectories in the westward direction,

as depicted in Figure 1.3.

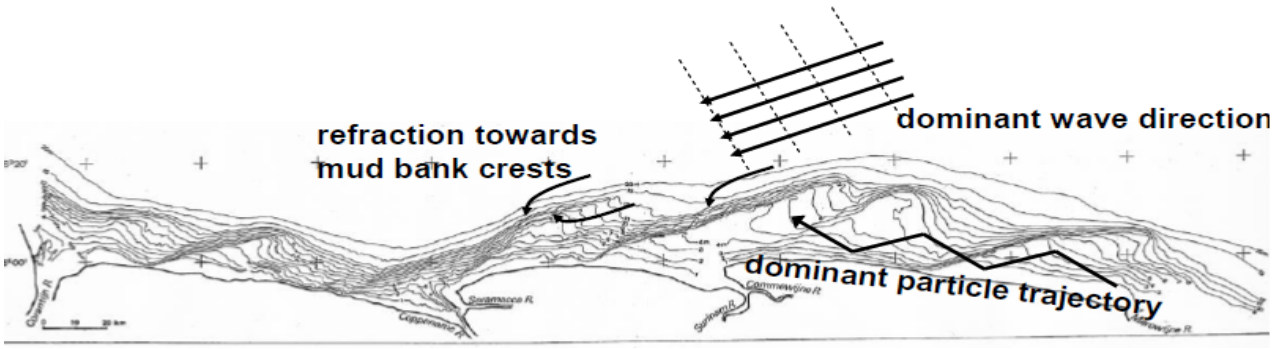

Figure 1.3: Nearshore bathymetry, Suriname (Augustinus, 1978). Thin black lines indicate locations with equal depth (isobaths) from 1-20 m . The thick zig-zag black line shows the dominant particle trajectory as a result of the perpendicular tidal currents and the along-shore Guiana current. The black arrows above the isobaths indicate the dominant wave direction. The small thick and curved black arrows show the refraction of incoming waves towards the crests of the mudbanks.

The local wave climate is characterized by swell waves originating from the Atlantic Ocean, wind waves generated by the trade winds and shorter waves developed also because of the Sea-Breeze modulation. Shoaling (increase of wave amplitude, decrease in propagation of wave energy, (Holthuijsen, 2007)) and refraction (turning of waves towards shallower water due to depth- or current-induced changes of the phase speed (Holthuijsen, 2007)) take place landward of the 20 m isobath (Nedeco, 1968).

Fresh water input from the Amazon river and the local rivers is important for the maintenance of the mangrove systems along the A-O coast. Due to the trade winds, the fresh water plume is kept close to the coast, within a narrow band of 30-50 km. The horizontal salinity gradients are generating a gravitational circulation with near-bed currents towards the coast (residual current). As a result, the fine sediments stay close to the shore, enhancing stratification and reducing vertical mixing (Augustinus, 1978).

1.2.2 Morphology

The mud supply transported from the Amazon river is maintained within a narrow band of 30 km offshore due to the prevailing trade winds, which do not allow the Guiana current to escape offshore. The mudbanks, are 10-30 km long, 10-20 km wide and they are spaced at intervals of 20-25 km along the coast. A sketch of mudbanks in Suriname coastal area is given in Figure 1.4.

The mudbanks in the coast of Suriname are shore-attached and triangularly shaped. Due to the wave attack from the NE, their eastern side is eroding (trailing edge). The waves, in combination with the longshore Guiana current, attack the mudbanks at their eastern side, and induce mobilization of the mud. The (fluid - mobilized) mud is transported towards the western side of the mudbanks (leading edge) and it is deposited there (Wells and Coleman, 1981; Froidefond et al., 1988). As a result, the thickness of the mudbanks increases towards the eastern side. Their crests are located in the direction NE-SW. The slope of the trailing edge is very mild while the slope of the lee side is much steeper. Although the mudbanks may reach up to 5-6 m of thickness, the part that is mainly associated with wave attenuation is the one that consists of fluid mud. This part may reach up to 2 m thickness.

The mudbanks prevent erosion of the coast, as they induce both depth-induced wave breaking and the fluid mud-induced wave damping since incoming waves refract on the slopes of the mudbanks and lose energy. The large migration rates of the mudbanks indicate that the area is highly dynamic. Some locations undergo bank phases, accompanied by coastal accretion, while other undergo inter-bank phases accompanied by coastal erosion. These processes have a periodic cycle of about 30 years. As a result, the wider area of Guiana basin is considered highly dynamic. Although high waves rarely occur in this area, these waves are strong enough to keep fine sediments in suspension (Wells and Coleman, 1981). During high tide the sediments are transported towards the coast, where an enhanced settling regime is created by mangrove traits such as roots. At some parts of the coast large mangrove forests are accompanied by long mudbanks in the nearshore area, while other parts are completely eroded.

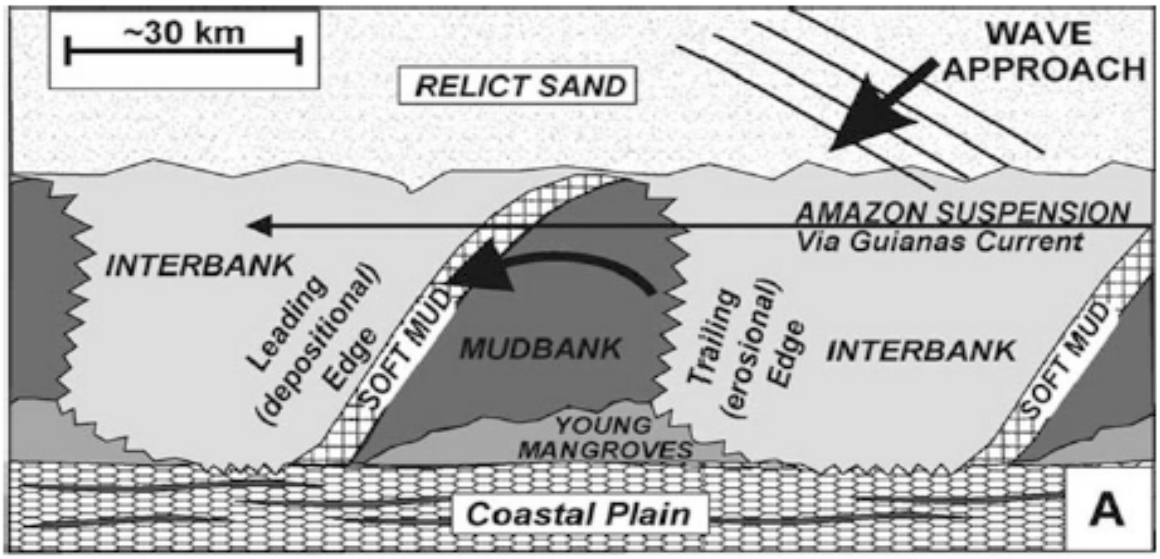

Figure 1.4: Sketch of a near shore area that is characteristic for the Amazon-Orinoco coast. Waves approach the coast from the NE direction, the same direction as that the wind is blowing from. The eastern side of the mudbanks is eroding while the western side is accreting. Between the mudbanks and the coastal plain there are mangrove forests. The areas between mudbanks is usually eroding; these are called interbanks areas (Toorman et al., 2018).

1.2.3 Potential problems in the muddy coastal area of Suriname

Sea level rise, flooding and coastal erosion are some of the high-risk issues encountered in the coast of Suriname and in the wider A-O area (Anthony, 2013). Many locations where mangrove forests used to thrive are now operating as fish ponds and polders. Coastal structures did not prove effective in an effort toprotecting the shoreline (Anthony and Gratiot, 2012). Without the contribution of the mangrove forests there will be significantly decreased sedimentation and wave attenuation and an increased need for continuous uninterrupted hard structures. However, hard structures do not allow for cross-shore sediment transport towards the shore. As a result, instead of protecting the coast, hard structures actually prevent sedimentation although they dissipate waves (Nedeco, 1968).

During the last years though, more problems are identified by Paul (2009). Since 1980, oil exploration activities take place. Environmental impact assessments have been conducted and established that, although no major negative environmental impacts will be observed, mitigating measures are

Figure 1.5: Erosion in the coast of Suriname. (Toorman et al., 2018).

needed so that the mangrove vegetation is able to further develop. At the same time, a quite common river-related issue arises. The need for deepening the Suriname's river lower levels in order for larger cargo vessels and cruisers to approach Paramaribo. Dredging will affect mangroves in a negative way, as it will suppress their roots, completely devastate parts of the forests, and increase tidal range. However, mangroves are vital for coastal protection, as they favor sedimentation and subsequent wave attenuation and prevent coastal erosion and flooding. Although mangroves do not thrive close to the channel, deepening of the channel can influence the passing mudbanks, which are directly related to the mangroves. Figure 1.5 shows part of the eroded coast of Suriname.

Moreover, sea level rise is one of the biggest risks for the Suriname coastal area, as it threatens the coast with extensive flooding and coastal degradation (Simpson et al., 2009). It is expected that the sea level rise in Suriname is close to the mean global average, 3.1 mm/year. In this case changes in currents and tidal parameters are predicted, leading to more severe coastal erosion, damaging of existing dykes and allowing salt water intrusion. Details about the impact of 1 up to 6 m sea level rise until 2100 are given respectively in Simpson et al. (2009) for the land area, population, urban and wetland area, agricultural and crop and plantation land, major tourism resorts, airports, road network and GDP in Suriname. The conclusion is that, even in the case of sea level rise of 1 m, Suriname is vulnerable due to its low-lying nature of the shoreline.

1.3 Overview of available knowledge and knowledge gaps

The coastal area between the Amazon and the Orinoco river is of great interest for many years. Various field observation studies took place along the Guiana basin starting from the 50s.

Nedeco (1968) aimed at providing information about the future accretion and erosion rates of the coast and the migration rates and direction of the mudbanks. During this study fundamental information was revealed about the combined action of the tidal and longshore Guiana currents, the

waves and the wind in the area. Augustinus (1978) studied the origins of the Suriname young coastal plain by making a detailed analysis of the existing sediment composition and the mechanisms that drive coastal accretion and erosion.

Recent studies, like the one from Anthony et al. (2008), involve modern technics: extraction of topographic data from satellite images and lidar data, and state-of-the-art field topographic survey systems. The objective of that study was the Macouria mudbank in French Guiana.

By now, more field studies took place. However, the modelling projects regarding the coastal area of Suriname are only few. Modelling projects are important in order to provide a more detailed insight on the hydrodynamics of the area, (long-term) predictions on the migration of the mudbanks, the evolution of the mangrove forests and facilitate and optimize human intervention in this area.

Toorman et al. (2018) reports that the KU Leuven morphodynamic model (based on the open source TELEMAC software) for the Suriname coast has been under development since 2005 with the help of some MSc thesis projects. Moreover, the parameterization from De Wit (1995), which discusses the two layer approach on wave attenuation over muddy beds, was implemented in the state-of-the-art wave numerical model SWAN by Winterwerp (2007) (for a case in Guyana).

De Wit's parameterization was optimized by Kranenburg (2008), where the DELFT parameterization is derived and implemented in SWAN. The corresponding version of SWAN is now called SWAN-Mud. In contrast to regular SWAN, SWAN-Mud can take into account (fluid) mud (Kranenburg, 2011). Different scientists tried in the past to develop a complete model that is able to calculate dissipation of wave energy by mud, while taking into account all the hydrodynamical processes that take place in a muddy environment. SWAN-Mud includes six different parametrizations: Gade: (Gade, 1958), Dalrymple: (Dalrymple and Liu, 1978), De Wit: (De Wit, 1995), Ng: (Ng, 2000), Guo: Guo (2002), DELFT: Kranenburg (2011). In a recent study by Beyramzade (2018), two more parameterization are implemented in a newer version of SWAN-Mud: (Macpherson, 1980) and (Liu and Chan, 2007). However, none of the SWAN-Mud versions has been tested in 2DH modelling projects. In both studies, Kranenburg (2011); Beyramzade (2018), 1D experiments are conducted.

This is one of the two knowledge gaps that is covered in this report. The second, relates to the general lack of modelling projects in the Suriname coastal zone.

1.4 Research objective and research questions

As a result of the problems that might occur in muddy coastal areas and of the knowledge gaps on the Suriname coastal zone discussed in the previous section, two major research questions have been developed in order to provide a deeper insight on the dynamics which dominates the area:

1. Can the state of the art numerical model SWAN-Mud simulate wave characteristics as are observed along the coast of Suriname and how are these wave characteristics influenced by the different wave dissipation formulations available?
In order to answer this question, SWAN-Mud is used for simulations in the coast of Suriname using a nearshore bathymetry from 2016 and by using the Kranenburg (2011) formulation as a reference case. Moreover some senitivity cases are studied, i.e. simulations take place with one other parameterization (Gade, 1958) and simulations for cases without a mud layer. The following wave parameters are analyzed and compared: wave height, direction, period, energy dissipation rate and near-bed orbital motion.

2. Can the commonly used numerical model Delft3D-FLOW successfully simulate currents found along the highly dynamic coast of Suriname?
Delft-3D FLOW is used in order to determine if the modelled water level and phase, depth-averaged velocity and direction correspond to values found in literature. Tests take place along a nearshore bathymetry from 2016.

The outline of this report is as follows: In Chapter 2, an extensive analysis and comparison of the different parameterizations used in SWAN-Mud is given and the equations that are solved by Delft3D-FLOW are explained. Moreover, a list of the experiments that are conducted is given and the model set up for each experiment is given. Results of the experiments are presented in Chapter 3 and a thorough discussion of the results is given on Chapter 4. Finally, the conclusions of this study are presented in Chapter 5.

Chapter 2

Materials and methods

2.1 Theoretical background

2.1.1 SWAN-Mud

2.1.1.1 Wave action balance

SWAN-Mud is the model which is used in order to answer the first research question. The original SWAN model (that does not include effects of mud) was first described by Booij (1999). SWAN is a third generation, phase-averaged, numerical, wave model and computes random, short-crested, wind-generated waves. SWAN-Mud (and every version of SWAN) solves the spectral wave action density equation at each grid point and time step, $N(\sigma, \theta, x, y, t)$. The wave action density balance equation is

$$\frac{\partial}{\partial t}N + \frac{\partial}{\partial x}c_{g,x}N + \frac{\partial}{\partial y}c_{g,y}N + \frac{\partial}{\partial \theta}c_{\theta}N = \frac{S_{tot}}{\sigma}, \tag{2.1}$$

where
σ is the relative radial frequency, in a frame of reference moving with the current velocity,
θ is the wave direction,
$N(\sigma, \theta)$ is the wave action spectral density, which is the energy spectral density $E(\sigma, \theta)$ divided by the relative frequency: $N = E(\sigma, \theta)/\sigma$,
$c_{g,x}$, $c_{g,y}$, c_{θ} are the propagation speeds of wave action in (x, y, θ) and
$\frac{S_{tot}}{\sigma}$ is the source term in terms of energy density.
The energy reads

$$E_{total} = \iint E(\sigma, \theta) d\sigma d\theta. \tag{2.2}$$

According to Holthuijsen (2007), the total energy density is proportional to the the root-mean-square wave height H_{rms}:

$$E_{total} = \frac{1}{8}H_{rms}^2 = \frac{1}{8}\left(\frac{1}{2}\sqrt{2H_s}\right)^2 = \frac{1}{16}H_s^2, \tag{2.3}$$

where:
H_s is the significant wave height which is the mean of the highest one-third of waves,
The first term on the left-hand of 2.1 side accounts for the local rate of change of action density in time. The second and the third term represent the propagation of wave action in the two-dimensional space, where $c_{g,x}$ and $c_{g,y}$ are the propagation velocities in x and y respectively. Finally, c_{θ} is the propagation velocity in the θ space.

The term S_{tot} consists of the sum of source and sink terms:

$$S_{tot} = S_{wind} + S_{wc} + S_b + S_{br} + S_{mud} + S_{nl}, \tag{2.4}$$

where:
S_{wind} accounts for generation of waves by wind,
S_{wc} represents dissipation by whitecapping, i.e. steepness induced wave-breaking,
S_b describes dissipation due to bottom friction,
S_{br} accounts for dissipation by depth-induced wave breaking,
S_{mud} accounts for dissipation by the (fluid) mud layer.
S_{nl} accounts for non-linear wave interactions.

Explicit expressions for the terms S_{wind}, S_{wc}, S_b, S_{br} and S_{nl} are given in Holthuijsen (2007). Various formulation for S_{mud}, dissipation of waves by the fluid mud layer, are used in this study (section 1.3). In case $S_{mud} = 0$, the regular SWAN version is being used.

A phase-averaged model does not calculate time series of sea surface elevations, but yields statistical properties of waves through the energy spectrum. SWAN follows an Eulerian approach. All processes can be described as sources and sinks in the basic wave action density spectrum.

2.1.1.2 Formulations for mud dissipation

There are six parameterizations implemented in SWAN-Mud. Gade (1958) was the first to build a two-layer viscous model in order to study the effects of waves propagating on a non-rigid bottom. Previous studies, e.g. Kranenburg (2008), indicate that the DELFT parameterization is the most advanced one. Besides the DELFT formulation, also the parameterizations from Gade (1958) will be discussed, as it consists of the basis for most of the future formulations that are developed.

The general model on which the two parameterizations are based, is a two-layer viscous fluid model where the top layer consists of water and the bottom layer consists of mud. Both fluids are considered Newtonian (incompressible). A sketch of this model is given in Figure 2.1.

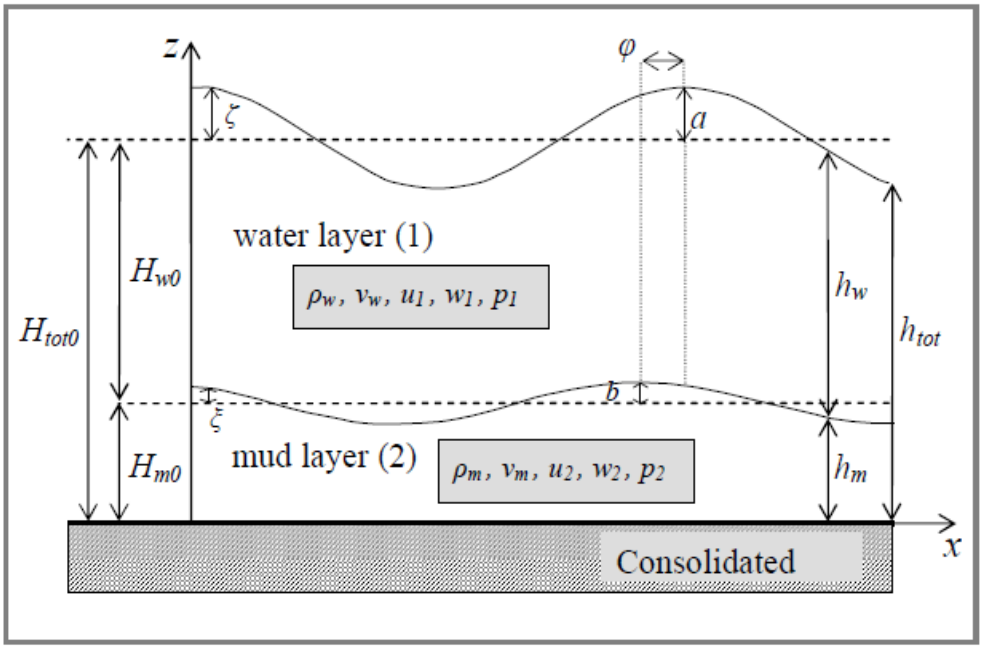

Figure 2.1: Sketch of the two layer fluid mud system (Kranenburg, 2008). The upper layer (1) is the water layer and the lower layer (2) is the mud layer. Beneath the mud layer, the bottom is assumed to be consolidated. Explanations of the variables are given in Table 2.1

Symbol	Description	Units
H_{w0}	Equilibrium height of water layer	m
H_{m0}	Equilibrium height of mud layer	m
H_{tot0}	Equilibrium height of total system	m
$h_w(x,t)$	Height of water layer	m
$h_m(x,t)$	Height of mud layer	m
h_{tot}	Height of total system	m
ζ	Displacement of water surface	m
α	Amplitude of water surface displacement	m
ϕ	Phase difference between surface and interface displacement	rad
ϕ'	Phase angle between surface and internal wave	rad
b	Amplitude of interface displacement	m
$\xi(x,t)$	Displacement of interface	m
ρ_w	Density of water	kg/m^3
ρ_m	Density of mud	kg/m^3
ν_w	Kinematic viscosity of water	m^2/s
ν_m	Kinematic viscosity of mud	m^2/s
u	Horizontal velocity in x-direction	m/s
w	Vertical velocity in z-direction	m/s
p	Pressure	N/m^2
ω	Wave (angular) frequency $2\pi/T$	rad/s
k	wavenumber	rad/m

Table 2.1: Variables used in Figure 2.1.

The model is based on the following assumptions.

- Fluid layers are considered to be of infinite horizontal extent.
- It is assumed that the mean current is zero.
- Motions of both fluids are free of divergence.
- The interface is assumed stable: no mixing between the two layers.
- Density and viscosity are assumed constant over a layer.
- The lower layer is assumed to lie on a rigid consolidated bed, not liquifiable by wave.
- Effects of the rotation of the earth are neglected.

The two-layer system is governed by the following equations:

$$\frac{\partial u_i}{\partial t} + \frac{1}{\rho_i}\frac{\partial p_i}{\partial x} - \nu_i\frac{\partial^2 u_i}{\partial x^2} - \nu_i\frac{\partial^2 u_i}{\partial z^2} = 0, \tag{2.5}$$

$$\frac{\partial w_i}{\partial t} + \frac{1}{\rho_i}\frac{\partial p_i}{\partial z} - \nu_i\frac{\partial^2 w_i}{\partial x^2} - \nu_i\frac{\partial^2 w_i}{\partial z^2} = -g, \tag{2.6}$$

$$\frac{\partial u_i}{\partial x} + \frac{\partial w_i}{\partial z} = 0. \tag{2.7}$$

These are, respectively, the horizontal momentum balance , vertical momentum balance and the continuity equation for layer i. In these equations, p is the total pressure and it consists of three contributions: The wave induced part, the hydrostatic part, and the ambient pressure (pressure at surface/ interface).
The boundary conditions read as follows.
At z=0, i.e. the bottom, a free slip boundary condition is applied:

$$u_2(x, 0, t) = 0, \tag{2.8}$$

$$w_2(x, 0, t) = 0. \tag{2.9}$$

At $z = h_m$, the height of the interface, kinematic and dynamic boundary conditions are imposed, i.e.,

$$w_1(x, h_m, t) = w_2(x, h_m, t) = \frac{\partial \xi(x, t)}{\partial t}, \tag{2.10}$$

$$\sigma_{zz2}(x, h_m, t) = \sigma_{zz1}(x, h_m, t), \tag{2.11}$$

$$\sigma_{xz2}(x, h_m, t) = \sigma_{xz1}(x, h_m, t). \tag{2.12}$$

Here, $\sigma_{zz} = -p + 2\rho_i\nu\frac{\partial w}{\partial z}$ is the normal component of the stress that acts at the interface and $\sigma_{xz} = \rho_i(\nu\frac{\partial w}{\partial x} + \nu\frac{du}{dz})$,the tangential component of the stress that acts at the interface.
At $z = h_{tot}$, particles at the surface need to follow the surface. This requires zero normal and tangential stresses.

$$w_1(x, h_{tot}, t) = w_2 = \frac{\partial \zeta(x, t)}{\partial t}, \tag{2.13}$$

$$\sigma_{zz1}(x, h_{tot}, t) = 0, \tag{2.14}$$

$$\sigma_{xz1}(x, h_{tot}, t) = 0, \tag{2.15}$$

This system allows for wave-like solutions. The displacement of the free surface and the interface, the (horizontal and vertical) velocity and the pressure in the two layers are described respectively by:

$$u_i(x, z, t) = \hat{u}_i(z)e^{i(kx-\sigma t)}, \tag{2.16}$$

$$u_i(x, z, t) = \hat{w}_i(z)e^{i(kx-\sigma t)}, \tag{2.17}$$

$$p_i(x, z, t) = \hat{p}_i(z)e^{i(kx-\sigma t)}, \tag{2.18}$$

$$\zeta(x, t) = \alpha e^{i(kx-\sigma t)}, \tag{2.19}$$

$$\xi(x, t) = be^{i(kx-\sigma t)}, \tag{2.20}$$

where k is the complex wavenumber with $k = k_r + ik_i$. The real part of the complex wavenumber introduces waves of sinusoidal form, while the imaginary part indicates the exponential decay of the waves, i.e. the energy loss per wavelength. Substitution of (2.16)-(2.20) into the equations of motion and boundary conditions yields a relation between the radian frequency σ and the complex wavenumber k. This allows calculation of k for a given wave frequency.

2.1.1.3 Gade:

In Gade's mathematical model the upper layer is inviscid, for both layers a shallow water approximation is used, pressure is assumed to be hydrostatic, vertical accelerations in both layers are neglected, and horizontal velocity in the upper layer is independent of depth. This model is applicable only in the case of shallow waters, i.e. $kh_w < \pi/10$. This constraint is the most important between the different assumptions Gade makes and restricts the applicability only to limited cases.

The dispersion relation of his model reads (equation I-26 (Gade, 1958)) :

$$k = \pm\sigma\left\{\frac{\left(1 + \Gamma\frac{H_{m0}}{H_{w0}}\right) \pm \sqrt{(1 + \Gamma\frac{H_{m0}}{H_{w0}})^2 - 4\gamma\Gamma\frac{H_{m0}}{H_{w0}}}}{2\gamma g\Gamma H_{m0}}\right\}^{1/2}, \tag{2.21}$$

where:

$$\Gamma = 1 - \frac{\tanh mH_{m0}}{mH_{m0}} \qquad m = (1 - i)\sqrt{\frac{\sigma}{2\nu_m}} \qquad \gamma = \frac{\rho_m - \rho_w}{\rho_w}, \tag{2.22}$$

and ν_m is the kinematic viscosity of mud.

Gade derived two important results about wave dissipation by the fluid mud layer, but in order to discuss them, it is first necessary to define the Stokes boundary layer thickness:

$$\delta_{BL} = \sqrt{\frac{2\nu_m}{\sigma}}, \tag{2.23}$$

The energy loss of a wave with wavenumber k_r due to a non-rigid bottom is given by:

$$S_{mud} = E\sigma g H_{w0} R \frac{b}{a} \sin(\phi - \phi'), \tag{2.24}$$

where

$$\frac{b}{a} = [(1 - gH_{w0}R\cos\phi)^2 + (gH_{w0}R\sin\phi)^2]^{1/2}, \tag{2.25}$$

and

$$\rho_w g S_{mud} = -\langle pw \rangle \Big|_{bed} \tag{2.26}$$

where the right hand side is the spectral energy density transfer from upper to lower layer, S_b is associated with the energy loss per time [m^2/s]
and R follows from eq. 2.21:

$$(\frac{k}{\sigma})^2 = Re^{-i\beta}, \tag{2.27}$$

with R is the amplitude and β is the argument of $(\frac{k}{\sigma})^2$. The right hand side should be multiplied with ω in order to correct for the original equation in Gade (1958).

According to Gade:
1. Most damping, i.e. exponential decay of the wave energy occurs if the mud layer thickness h_m is approximately equal to 1.2 times the Stokes boundary layer thickness, i.e. $h_m = 1.2\delta_{BL}$.
2. The internal wave at the interface between the two layers will always lag behind the surface wave; which means that there will always be transport of energy from the upper to the lower layer. As a result, the larger the phase difference, the larger the k_i, the larger the dissipation. The above-explained model is implemented in SWAN-Mud.
3. The strong constraint of the model is its area of applicability, i.e. the fact that it is valid only in the case when the internal wave satisfies the shallow water limitation. This is indeed a limiting factor in the case of Suriname. The mud layer in this area is maintained in the first 15-30 km from the shore, where the water depth goes up to 20 m and the mud layer up to 2 m. The shallow water limitation (Holthuijsen, 2007) is

$$k_{r,int} H_m < \frac{\pi}{10}$$

where $k_{r,int}$ is the real part of the complex internal wavenumber. The speed of the internal wave is much smaller than that of the external wave, since wave speed in shallow waters is $c = \sqrt{gH}$ where H is H_w for the external wave and H_m for the internal. The real part of the wavenumber k is computed according to $k_r = \frac{2\pi}{Tc}$. The phase speed c of the internal wave is smaller and this will make $k_{r,int}$ larger compared to the external wave.

2.1.1.4 DELFT

The DELFT dispersion relation is explained in Kranenburg (2008) and Kranenburg (2011). The formulation allows for arbitrary thicknesses of both the water layer and the mud layer. The DELFT dispersion relation reads

$$\omega^4\Big(\frac{\cosh(kH_{w0})\cosh(mH_{m0})}{k} - \frac{\rho_w}{\rho_m}\frac{\sinh(kH_{w0})\sinh(mH_{m0})}{m} + h_{m0}\frac{\rho_w}{\rho_m}\sinh(kH_{w0})\cosh(mH_{m0})\Big)$$
$$+ \omega^3 2ik\nu_m\cosh(kH_{w0})(\cosh(mH_{m0}) - 1)$$
$$+ \omega^2 g\Big(\frac{k}{m}\cosh(kH_{w0})\sin(H_{m0}) - kH_{m0}\cosh(kH_{w0})\cosh(mh_{m0}) - \sinh(kH_{w0})\cosh(mH_{m0})\Big)$$
$$+ \omega^2 gk^2\nu_m\sinh(kH_{w0})(1 - \cosh(mH_{m0}))$$
$$+ g^2k^2\Big(H_{m0}\frac{\rho_2 - \rho_1}{\rho_2}\sinh(kH_{w0})\cosh(mH_{m0}) - \frac{\rho_m - \rho_w}{\rho_m}\frac{\sinh(kH_{w0})\sinh(mH_{m0})}{m}\Big) = 0. \tag{2.28}$$

In this case, the energy dissipation term due to the mud layer is

$$\frac{S_{mud}}{E} = -\sigma\frac{\mathrm{Re}\{p_{1(z=H_{m0})}\}}{\rho_1 g\alpha}\frac{b}{\alpha}\sin\phi, \tag{2.29}$$

where

$$p_{1(z=H_{m0})} = \rho_1\alpha g\cos(kH_{w0}) - \frac{\rho_1\alpha\sigma^2}{k\sinh(kH_{w0})}. \tag{2.30}$$

In this formulation, the regular bottom friction, S_b, is present together with mud-induced dissipation. The model computes both, but uses only the largest of the two.

To sum up, equation 2.4 becomes:

$$S_{tot} = S_{wind} - S_{wc} - S_{br} - max\big[S_b, S_{mud}\big] - S_{nl}. \tag{2.31}$$

2.1.2 Delft3D

Delft3D-FLOW is the model which is used in order to answer the second research question, i.e. to assess to what extent currents in the Suriname coastal zone can be simulated with a hydrodynamic model. In the version of Delft3D-FLOW that is 2D the over the full depth-averaged shallow water equations are solved. The equations are derived from the three-dimensional Navier-Stokes equations for incompressible flow under the assumption of hydrostatic balance and constant density. In the open boundaries (west, north, east) water level is imposed, as obtained from tide tables in Delft-Dashboard (manual Delft3D-FLOW), and at the closed boundary no slip boundary conditions are imposed.

$$\frac{\partial u}{\partial t} + u\frac{\partial u}{\partial x} + v\frac{\partial u}{\partial y} - fv = -g\frac{\partial\zeta}{\partial x} - \frac{\tau_{bx}}{h} + \frac{1}{h}\Big(\frac{\partial}{\partial x}\Big(\nu_e h\frac{\partial u}{\partial x}\Big)\Big) + \Big(\frac{\partial}{\partial y}\Big(v_e h\frac{\partial v}{\partial y}\Big)\Big) + \frac{\tau_{wx}}{\rho h}, \tag{2.32}$$

$$\frac{\partial v}{\partial t} + u\frac{\partial v}{\partial x} + v\frac{\partial v}{\partial y} + fu = -g\frac{\partial\zeta}{\partial y} - \frac{\tau_{by}}{h} + \frac{1}{h}\Big(\frac{\partial}{\partial x}\Big(\nu_e h\frac{\partial v}{\partial x}\Big)\Big) + \Big(\frac{\partial}{\partial y}\Big(\nu_e h\frac{\partial v}{\partial y}\Big)\Big) + \frac{\tau_{wx}}{\rho h}, \tag{2.33}$$

$$\frac{\partial\zeta}{\partial t} + \frac{\partial(hu)}{\partial x} + \frac{\partial(hv)}{\partial y} = 0. \tag{2.34}$$

Here, u, v represent the depth averaged velocity components in x, y direction, ρ is the water density, ζ is the sea surface elevation, f is the Coriolis parameter and g is the gravitational acceleration. Furthermore, ν_e is the horizontal eddy viscosity and τ_{bx} and τ_{by} is the bed shear stress where

$$\tau_{bx} = \rho C_d (u^2 + v^2)^{1/2} u \qquad \tau_{by} = \rho C_d (u^2 + v^2)^{1/2} v \tag{2.35}$$

and C_d is the drag coefficient. The latter is calculated according to $C_d = g n^2 / h^{1/3}$ where n is the Manning coefficient (manual Delft3D-FLOW).

2.2 Model set up

In this section the model settings and the experiments performed in order to answer the two research questions will be explained. More particularly, the two model domains are presented, the input parameters and the boundary conditions are explained, a list of all the experiments is given and finally the methods to analyse the results are discussed.

2.2.1 Bathymetry

Due to the nature of the two research questions, different models will be used in each case. However, the same bottom topography is used for both questions in order to explicitly study the effect of waves and currents in each bathymetry. In this study, the bathymetry from 2016 is used. The measurements

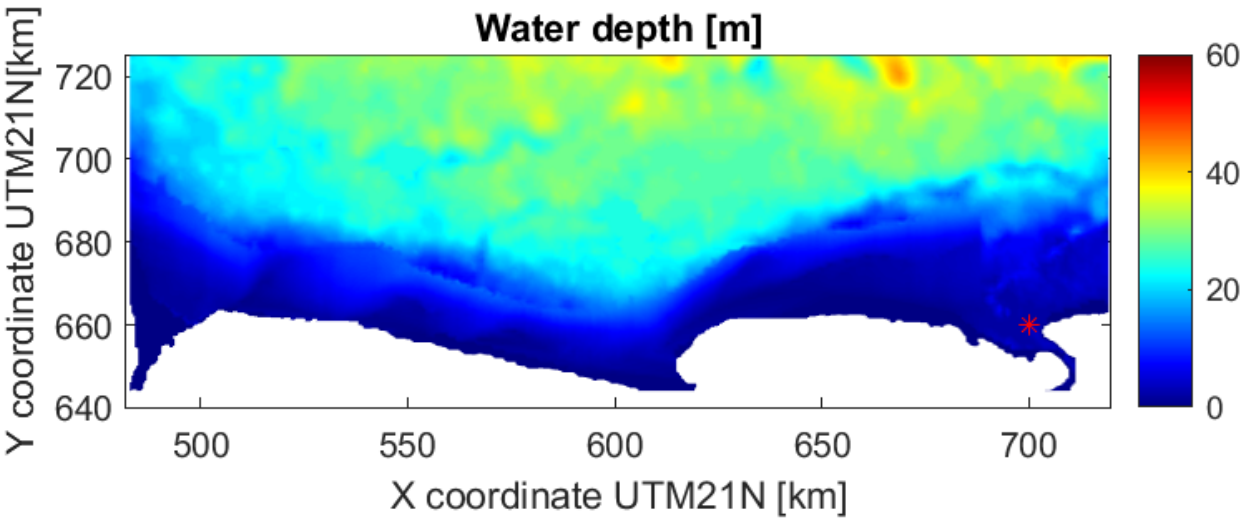

Figure 2.2: Bathymetry from 2016 (nearshore) and GEBCO dataset (offshore). The red asterisk indicates the location of a local tidal station 'Surinamrentriho'.

are echosounds at 38 KHz (according to the Maritime Authorities website [1]).

The nearshore bathymetric data are not enough in order to design model grids with sufficiently large dimensions. This aspect of the model set-up will be further explained later. As a result, offshore data are needed. However, a high degree of accuracy in the offshore data is not necessary, as the mudbanks, one of the most important features of the area, are located in the nearshore bathymetry. So the main utility of the offshore data is to serve numerical aspects of the experiments. Consequently the GEBCO bathymetry dataset (GEBCO) will be used in order to obtain offshore data and combine them with the onshore data of the bathymetry from 2016. The combined bathymetry from 2016 and the GEBCO dataset is presented in Figure 2.2.

[1] https://www.mas.sr/12-nautical-management/9-hydrography-fairway-management

2.2.2 Design of the mudbanks

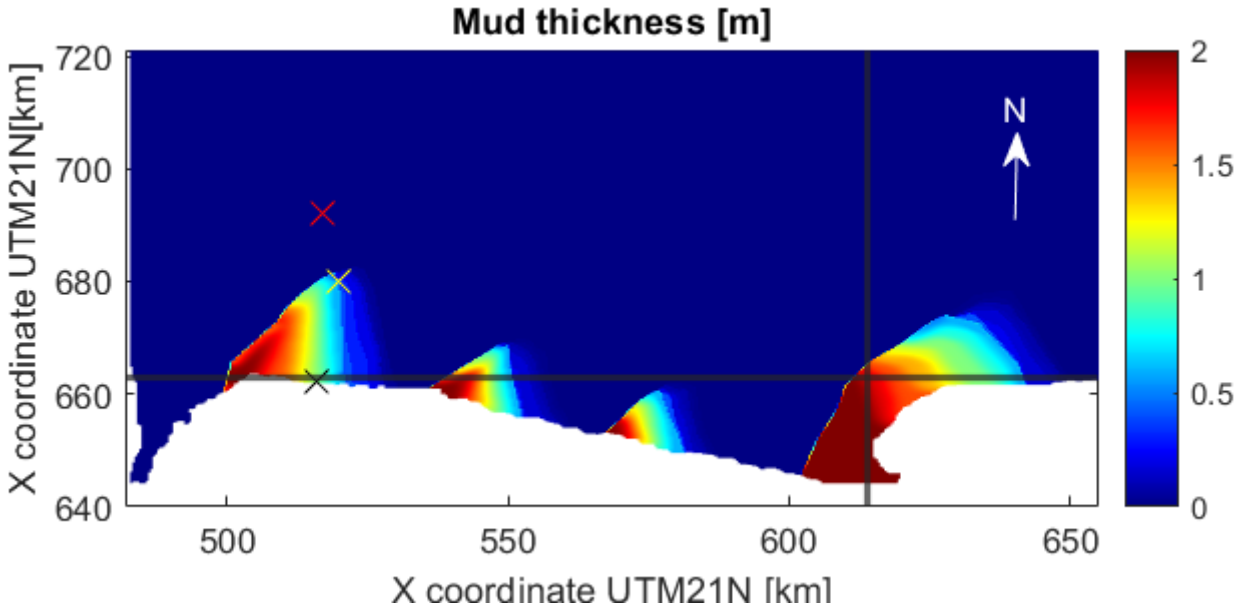

Figure 2.3: Mud layer thickness used for simulations with SWAN-Mud. Four mudbanks are presented with increasing thickness from east to west. The location of the mudbanks is based on the bathymetry in Figure 2.2. The horizontal and vertical black lines indicate along- and cross-shore sections which are analyzed in Section 3.1. The crosses indicate the locations where the wave spectra are computed.

No measurements are available of the shape, the thickness, and the composition of the mudbanks accompanying the bathymetry observations on 2016. Therefore the design of the mudbanks for the purposes of this report is based on a literature review (section 1.2.2) and discussion with experts on the field.

As already discussed, the mudbanks are shore-attached and they are triangularly shaped. The eastern side of the mudbanks is of low thickness, which is increasing towards the western side. It is assumed that the location of the mudbanks is depicted in the bathymetry (thick, triangular shaped, shore-attached patches). Figure 2.3 shows the thickness of the mudbanks.

2.2.3 SWAN-Mud Model

The grid that is used for the experiments in SWAN-Mud is generated based on the bathymetry data availability, using two pre-processing tools of the model Delft3D, RGFGRID and QUICKIN. A distinction should be done between the physical domain, and the overall computational grid. The first represents the area of interest, where the focus of the study lies and it is usually smaller than the computational grid. The latter, is large enough in order to facilitate valid numerical simulations and correct application of the boundary conditions. In Figure **??** the grid is projected in the world map of Delft-Dashboard in order to get a better view of the size and the location of the model domain.

The smaller, physical domain consists of grid cells with dimensions of 400 m by 150 m (alongshore by cross-shore direction) and it covers an area of approximately 180 by 57 km (alongshore by cross-shore direction). The larger domain consists of grid cells with dimensions 400 m by 150 m and it covers an area of about 230 km by 87 km .

In order to study the effect of the mudbanks on waves, two experiments are performed. In the first case, the system is forced with a large value of significant wave height of 4 m in the northern

and eastern boundaries, where a wavefield that satisfies a given energy density spectrum imposed. Extending the boundaries across the whole northern and eastern boundary, a shadow effect is avoided. At the same time, a constant wind of 12.5 m/s is initialized. This is the case of extreme conditions. In the second case normal conditions are imposed. In this case only a typical wind velocity is imposed that allows for wave generation.

In both cases, the same physical processes are activated. Swan-Mud is running in third generation mode, which activates a wind input, whitecapping (steepness-induced wave breaking) and quadruplets (nonlinear wave-wave interactions). Moreover, depth-induced wave breaking is activated. The mud layer is spatially varying and is inserted in the model as an input file similar to the one where the bathymetry is inserted. The default setting of a minimum water depth of 0.05 m is deactivated. This is important because in the case of the mud layer thickness, 5 cm of mud are enough to dissipate waves even in deep waters. Directions are relative to North (clockwise) (nautical direction is set). The spectral directions cover a full circle. There are 35 discrete frequencies which are used in the calculations, between 0 Hz and 1 Hz. Finally, the model runs in a stationary mode. The most important model settings are summarized in Table 2.2.

In the reference case DELFT parameterization is used, and in the sensitivity tests, Gade is used. Moreover, a case without the mud layer is tested. All these experiments are repeated for both the normal and extreme conditions with exactly the same model setup as described earlier and in Table 2.2, excluding the mud layer.

2.2.4 Delft3D Model

Regarding the second research question, a more complicated process is needed in order to accurately represent the tidal currents in the two domains. In this case, the process of nesting takes place. For this reason, a larger overall grid is needed in order to impose tidal astronomical boundary conditions at its offshore boundaries. In the overall grid, observation points are located in the offshore

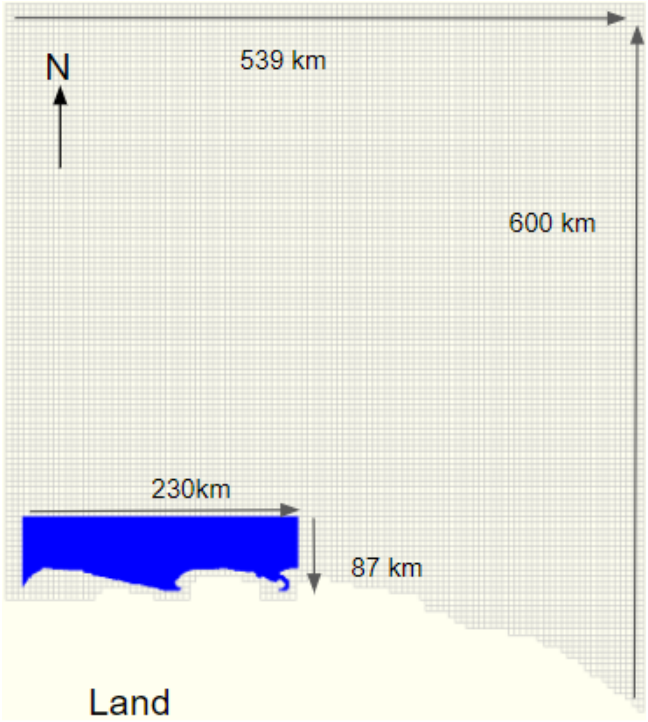

Figure 2.4: Grid of the physical domain (blue area) and overall domain (dashed area).

Parameter	Description	Extreme conditions	Normal conditions
$H_{s,bound}$	Forcing significant wave height	4 m	-
T	Period significant wave height	10 s	-
Dir H_s	Direction significant wave height	45°	-
DD	Directional spreading significant wave height	25°	-
	Boundaries for forcing $H_{s,bound}$	north, east	-
W_s	Wind speed	12.5 m/s	12.5 m/s
Dir W_s	Direction wind speed	45 °	45 °
ν_m	Mud viscosity	0.001 m^2/s	0.001 m^2/s
ρ_m	Mud density	1400 kg/m^3	1400 kg/m^3
ρ_w	Water density	1000 kg/m^3	1000 kg/m^3

Table 2.2: Model setup of SWAN-Mud for normal and extreme wave conditions. Experiments without mud take place for the same normal and extreme wave conditions by switching off the presence of mud.

boundaries of the physical domains. In that way timeseries with tidal conditions are obtained for the physical domain. These timeseries are used in order to force the smaller physical domain.

Parameter	Overall domain	Physical domain
Time step	5 min	60 s
Grid cell size	5x5 km	400x180 m
Tidal forcing	Astronomical conditions	Timeseries
Wind speed W_s	12.5 m/s	12.5 m/s
Dir W_s	45 °	45 °
Bottom roughness	0.012 $m^{-1/3}/s$	0.012 $m^{-1/3}/s$
Water Density	1000 kg/m^3	1000 kg/m^3

Table 2.3: Variables for experiments in Delft3D-FLOW during the process of nesting. Overall and physical domain are shown in Figure 2.4.

More particularly, the larger, overall domain is forced with astronomical tidal conditions using datasets from Delft-Dashboard and a constant wind. The physical domain consists of grid cells with dimensions of 400 m by 150 m and it covers an area of approximately 230 by 57 km. In the overall domain, the grid cells are of size 5 by 5 km and the area is approximately 600 km long cross-shore (see Figure 2.4 in the west and 530 km long alongshore. The input parameters are listed in Table 2.3.

The model was calibrated by tuning the value of the roughness coefficient. A sensitivity analysis takes place in order to determine the bottom roughness coefficient that best fits the model set-up. Timeseries from the local tidal stations (red dots in Figure 2.2) are compared to the model output timeseries. The roughness coefficient that corresponds to best fit determines the simulations which will be used in order to perform a water level and velocity harmonic analysis.

2.2.5 Design of experiments

A complete list of all the experiments that take place throughout this study is given in Table 2.5.

Parameter	Overall domain	Physical domain
Forcing	Timeseries tides	Wind
Wind speed W_s	12.5 m/s	12.5 m/s
Dir W_s	45 °	45 °
Bottom roughness	0.012 $m^{-1/3}/s$	0.012 $m^{-1/3}/s$
Mud Density	-	1400 kg/m^3
Water Density	1000 kg/m^3	1000 kg/m^3

Table 2.4: Variables for experiments in Delft3D-FLOW. Overall and physical domain are shown in Figure 2.4.

Experiment No.	Description	Details
Experiment 1	SWAN-Mud: DELFT formulation, Extreme conditions	Table 2.2
Experiment 2	SWAN-Mud: Gade formulation, Extreme conditions	Table 2.2
Experiment 3	SWAN: Extreme conditions	Table 2.2
Experiment 4	SWAN-Mud: DELFT formulation, Normal conditions	Table 2.2
Experiment 5	SWAN-Mud: Gade formulation, Normal conditions	Table 2.2
Experiment 6	SWAN: Normal conditions	Table 2.2
Experiment 7	Delft3D-FLOW: Extreme conditions	Table 2.4

Table 2.5: List of experiments with SWAN-Mud and Delft3D-FLOW.

2.3 Methods to analyse model outputs

In this section, a short overview of the methods to analyze the model outputs is presented.

For Experiments 1-6, spatial plots of significant wave height, wave period, total dissipation, wave direction and orbital velocity are analyzed. Furthermore, alongshore and cross-shore sections give a more detailed analysis of the above mentioned variables and of the dissipation sources. Finally, wave spectra (Holthuijsen, 2007) are analyzed for different locations in the area of interest.

Results from Experiments in Delft3D-FLOW are initially analyzed through the sensitivity analysis described in Section 2.2.4. Sea surface elevation data are compared with observations from tidal stations in the area graphically and the Root Mean Square Error (RMSE) between observations and model outputs is computed. The RMSE is computed according to

$$RMSE = \sqrt{\frac{\sum_{t=1}^{N}(x_{t,model} - x_{t,obs})^2}{N}} \tag{2.36}$$

where:
N is the total number of data points which is the same as the number of timesteps,
$x_{t,model}$ indicates data points of the model outputs at time t,
$x_{t,obs}$ indicates data points of the observations at time t.
RMSE is a measure of the skill of the model. The smaller the RMSE, the better the model. RMSE has the same units as the tested variable, e.g. units of [m] in case of sea surface elevations.

According to the sensitivity analysis results, the model set up which gives the most representative data is analyzed. Harmonic analysis of the water level and of the depth averaged velocity takes place (Pugh and Woodworth, 2014). The idea of water level harmonic analysis is to reconstruct the water level signal by fitting a number of tidal constituents to the timeseries obtained by the model output. The harmonic analysis in both cases is performed according to Pawlowicz et al. (2002). We can model

a tidal signal as a superposition of a number of tidal waves,

$$\hat{\zeta}(t) = Z_0 + \sum_{m=1}^{M} Z_m \cos(f_m t - \varphi_m). \tag{2.37}$$

Here,
Z_0 is the mean water level,
$\hat{\zeta}$ is the water level elevation,
M is the total number of tidal components,
f_m is the frequency of component m,
Z_m is the amplitude,
φ_m is the phase and t is time.
We choose the number of components M and we know each of the frequencies f_m. The unknowns are then Z_m and φ_m. We find the values of these parameters by fitting the model on the data with a least squares approach i.e. by minimizing the error described in Equation 2.36, where $x_{t,model}$ is in this case the reconstructed model time series, $\hat{\zeta}(t)$ and $x_{t,obs}$ is in this case the model output timeseries from Delft3D.

The harmonic analysis is performed using the following tidal constituents: M_2, the principal lunar semidiurnal tide with a period of 12.42 hr, its first overtide M_4 and the residual current M_0, the principal solar semidiurnal tide S_2 with a period of 12 hr and for the lunar diurnal tide K_1 with a period of 23.93 hr.

Next, the depth-averaged velocity is analyzed. A similar approach to the water level harmonic analysis is followed in order to analyse the current velocities. In that way, it is possible to obtain the velocity amplitudes of the zonal and meridional components and phases of the above-mentioned tidal constituents. The current velocity vector of each tidal constituent follows an ellipse in time. A full rotation of the velocity vector takes place during each tidal cycle. The semi-major axis of the ellipse represents the maximum velocity within one period of the tidal constituent and the semi-minor axis represents the minimum velocity. As a result, the main direction of the tidal current is related to the major axis of the ellipse. Spatial maps of water level for the most important tidal constituents are presented. The main direction of the tidal current for the tidal constituent M_2 is presented with a spatial map of the tidal ellipses. Finally, a plot with iso-phase lines of M_2 is explained.

Chapter 3

Results

Prior to testing SWAN-Mud in the coast of Suriname, it is important to determine in what extent SWAN-Mud is able to reproduce results from previous related studies, i.e. the following studies: De Wit (1995), Winterwerp (2007) and Kranenburg (2011). This analysis takes place in Appendix A and it is crucial in order to establish the validity of the model. Chapter 3 analyzes the results of all the experiments discussed in section 2.2. More particularly the results from the experiments with SWAN-Mud for extreme conditions are analyzed in Section 3.1.1, and for normal conditions in Section 3.1.2. The results from Delft3D-FLOW are explained in Section 3.2.

3.1 Experiments with SWAN-Mud

3.1.1 Extreme conditions

The model set up for the experiments during extreme conditions is described in Table 2.2 and the mudbanks are designed according to the description given in Section 2.2.2. The water depth is found in Figure 2.2 and the mud layer thickness is shown in Figure 2.3. In the same figure the black lines represent cross- and alongshore sections and the crosses represent locations where the wave spectra are calculated.

Prior to a detailed analysis of the cross- and alongshore sections, it is meaningful to assess the general reaction of the system in the case where the mud layer is present and in the case without one. For this, spatial plots of significant wave height, wave period, and total disipation are given in Figure 3.1 and wave direction and orbital velocity in Figure 3.4 with DELFT and Gade formulation and in the case without mud. The above mentioned parameters are analysed across along- and cross-shore sections in Figures 3.5 and 3.2. The dissipation sources are analysed across the same alongshore and cross-shore sections in Figures 3.6 and 3.3. Both the figures with the alongshore and the figures with the cross-shore sections offer a more detailed look of how wave characteristics vary between the different formulations in the offshore part of the domain and also in the nearshore part. However it should be taken into account that regarding the alongshore section, the distance of the shore compared to this alongshore section varies. The aim of studying an alongshore section is to study the variability along the coastline where depositional parts alter with erosional parts. At the right in Figures 3.5 and 3.6, it is the eastern edge of the coastline and at the left it is the western edge. There are three mudbanks along the coastline, with increasing thickness from east to west.

The significant wave height decreases instantly as soon as the waves meet the mud layer when using both formulations DELFT and Gade, Figure 3.1. The first column of this figure clearly shows larger wave heights offshore (red shades) compared to the locations of mudbanks (blue shades). The lower, blueish, values (0-2 m) closer to the coast are shaped like triangles, indicating the presence of

the mudbanks. In case of Gade H_s decreases already at the 690 km offshore (acquires yellow colour) in the most western mudbank, while with Delft formulation this happens approximately at the 680 km. This is an indication that Gade formulation overestimates wave dissipation compared to DELFT formulation. In case without mud, the triangular shape of yellowish colours is much less pronounced indicating that waves dissipate later.

Regarding the pattern of wave period, shown in Figure 3.1, results with DELFT formulation are in agreement with Winterwerp (2007) (see Appendix A) while results with Gade formulation are in agreement with Wells and Coleman (1981) (see Table 1 in mentioned paper). In the reference case, with DELFT formulation the period is decreasing while in the case of Gade, the wave period is increasing. Although it has been established that Gade's formulation is not valid for the coast of Suriname, it is not the first time a pattern like this is observed. Wells and Coleman (1981) observed after measurements in Suriname that the wave period between two stations 11 km and 4 km from the shore is increasing. This is explained by the attenuation of higher frequency waves in an earlier stage. In the case without mud the pattern is as expected, the wave period is decreasing towards the coast, as the bathymetry is already elevated in the location of the mudbanks.

The spatial plots of total dissipation show negligible dissipation ($0 - 0.2 \cdot 10^{-3}$ m^2/s) in the offshore part of the area (720 – 690 km cross-shore) for all three cases because there are no differences in this part. The only source of dissipation in this part is whitecapping. This is shown in the cross-shore section in Figure 3.3. Taking into account the locations of the mudbanks in Figure 2.2.2, we can see that the pattern in wave dissipation between 650 – 640 km alongshore is the same as the waves approach from the north and the east and are not affected by the presence of the mudbanks already. However, in the locations between the mudbanks (605–680 km, 565–555 km , 540–545 km alongshore) and after the mudbanks (480 – 500 km alongshore) the wave dissipation is similar but not exactly the

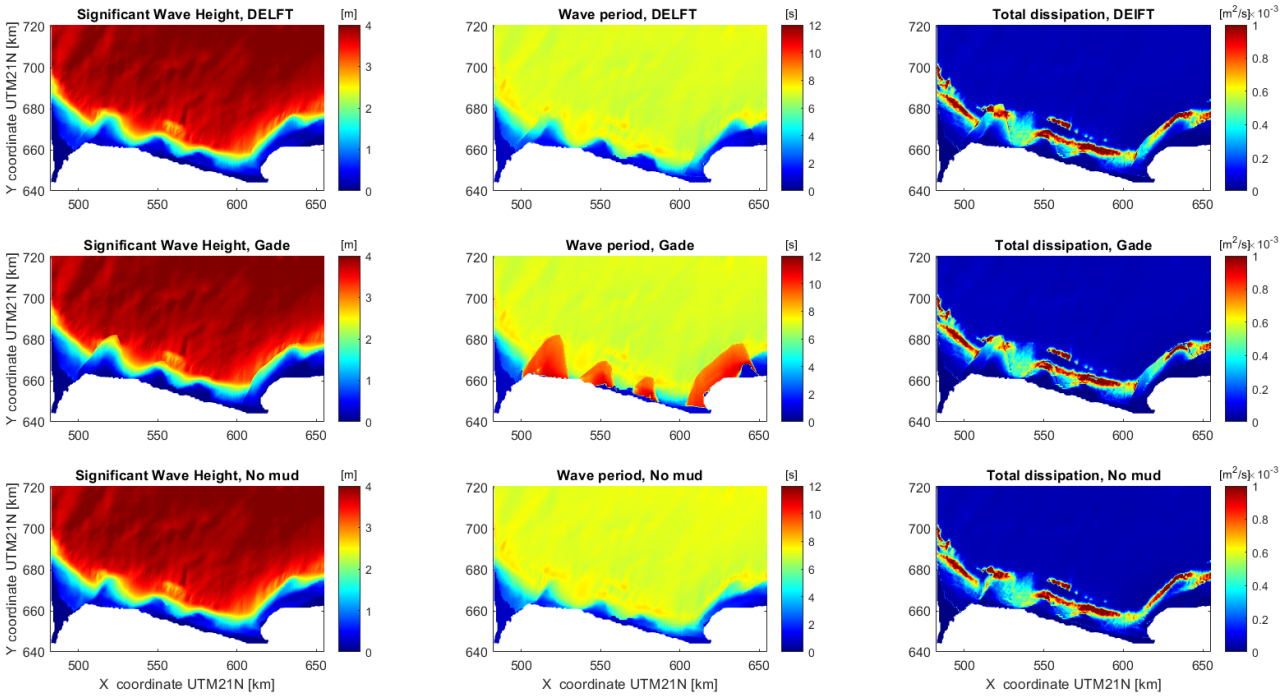

Figure 3.1: Spatial plots for significant wave height [m] (1st column), wave period [s] (2nd column) and total dissipation [m^2/s] (3rd column). In the first row the results with DELFT formulation are presented (Kranenburg, 2011), in the second the results with Gade formulation (Gade, 1958), and in the last row the results for the case without mud are presented.

same, as waves that approach from the east are affected by the mudbanks. Wave dissipation in these locations is mainly due to wave-breaking as indicated in the cross-shore and alongshore sections in Figures 3.3 and 3.6. In the cases where mud is present wave dissipation starts earlier compared to the case without mud. For example between 540 – 550 km alongshore, dissipation starts at the 680 km cross-shore in cases with mud, and at the 670 km in the case without mud. According to the detailed analysis of the dissipation sources in Figure 3.3 mud induced dissipation increases sharply as soon as the waves approach to the mudbanks. From that, we can conclude how effective mud is in dissipating wave energy. In the same Figure we can that mud-induced dissipation is in the same order of magnitude as dissipation due to wave breaking (10^{-4} m^2/s). The sharp increase and decrease in dissipation due to whitecapping with Gade formulation could be a model error.

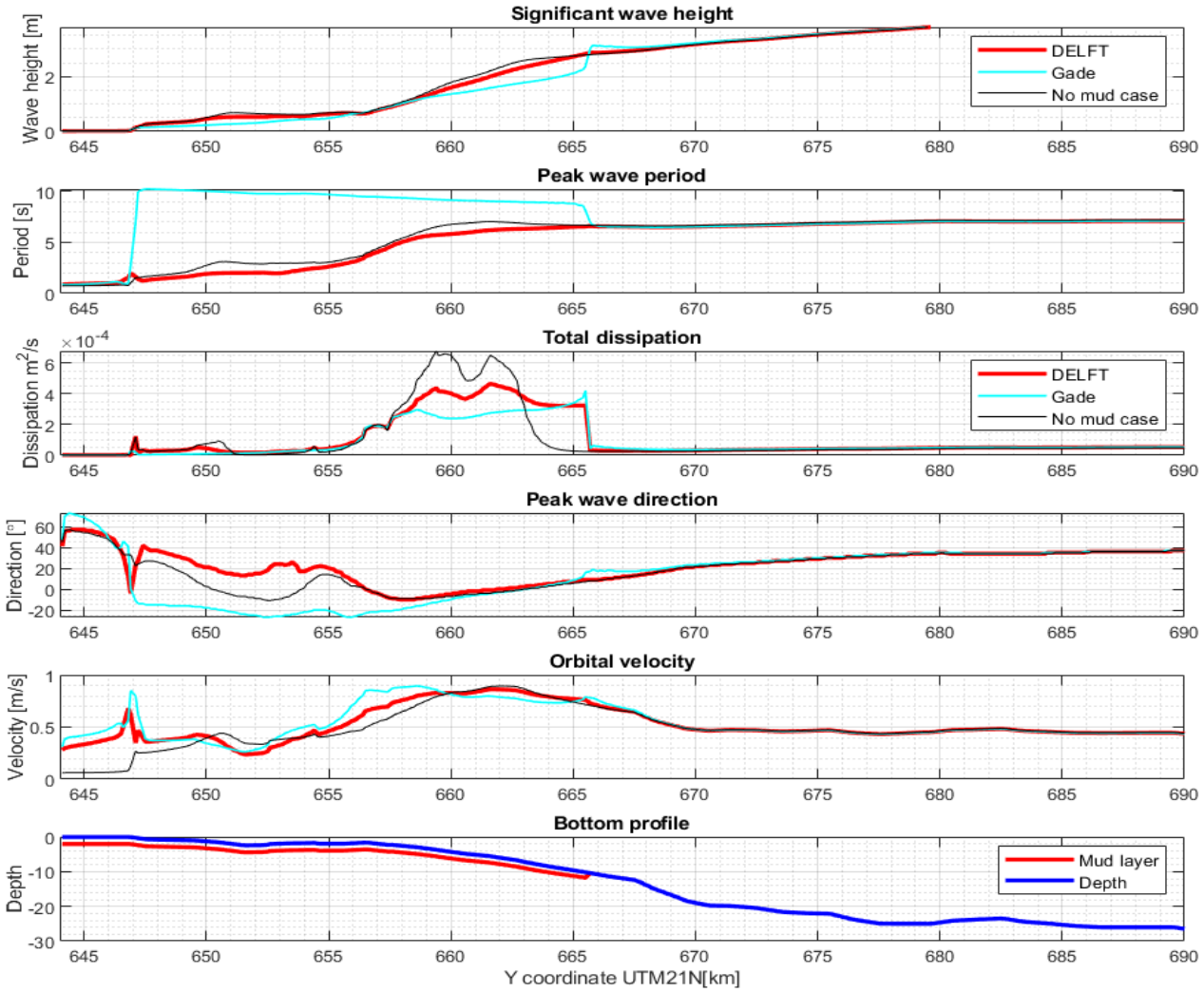

Figure 3.2: Cross-shore section for the bathymetry indicated in Figure 2.3. The lower plot shows the water depth profile (blue line) and the mud patches (red lines). From top to bottom, the first plot shows the significant wave [m], the second total dissipation [m^2/s], the third peak wave period [s], the fourth peak wave direction [°] and the fifth orbital velocity [m/s]. The red line indicates DELFT formulation, the cyan line Gade formulation and the black line the case without mud.

In the second column of Figure 3.4 the pattern of the amplitude of the near-bed wave velocity is shown. It is expected to increase in the locations of small water depths (Holthuijsen, 2007). Indeed, it increases from the 680th km offshore towards the shore but only until waves meet the mud layer. After that, orbital velocity decreases significantly, as waves have dissipated. For the case without a

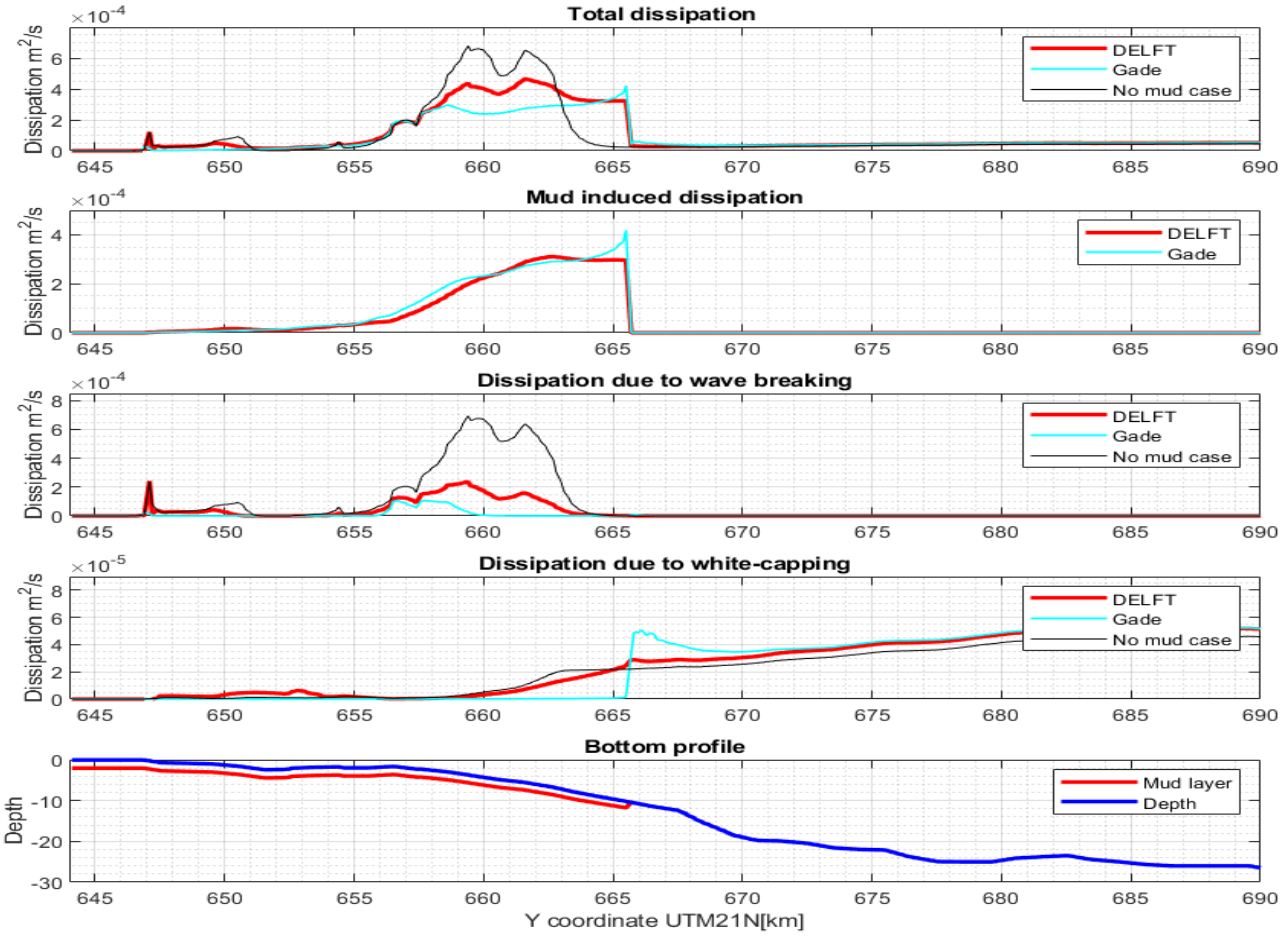

Figure 3.3: Cross-shore section for the bathymetry indicated in Figure 2.3. The lower plot shows the water depth profile (blue line) and the mud patches (red lines). From top to bottom, the first plot shows total dissipation [m^2/s], the second mud induced dissipation [m^2/s], the third wave breaking induced dissipation [m^2/s] and the fourth dissipation from whitecapping [m^2/s]. The red line indicates DELFT formulation, the cyan line Gade formulation and the black line the case without mud.

mud layer, the orbital velocity also reduces towards the coastline, but it does not gain the low values as in the cases with mud (see Figures 3.2, 3.5). The orbital velocity in case of DELFT and Gade is not zero at the coastline, as it is in the case without mud. This probably an error of the model.

The wave spectra in Figure 3.7 shows in which frequencies the wave energy is distributed. Starting from offshore (see Figure 2.2.2), low frequency waves (swell waves, $T = 10$ s) acquire most of the energy in all three cases. A small amount of the energy is distributed among waves of frequency 0.1-0.25 Hz as well, although waves were forced with a period of 10 s in the boundaries. The small shift towards larger frequencies can be explained by dissipation due to whitecapping (see Figure 3.2 and from the presence of the wind waves. At the starting point of the mudbanks, waves in DELFT formulation lost more energy compared to the case without mud. The reason is that in this case waves dissipate more due to the presence of the mud layer. Although there is loss of energy, there is not a pronounced shift in larger frequencies. In case of Gade the loss of energy is larger, as expected, since in the beginning of the mudbanks, significant wave height is lower and energy dissipation

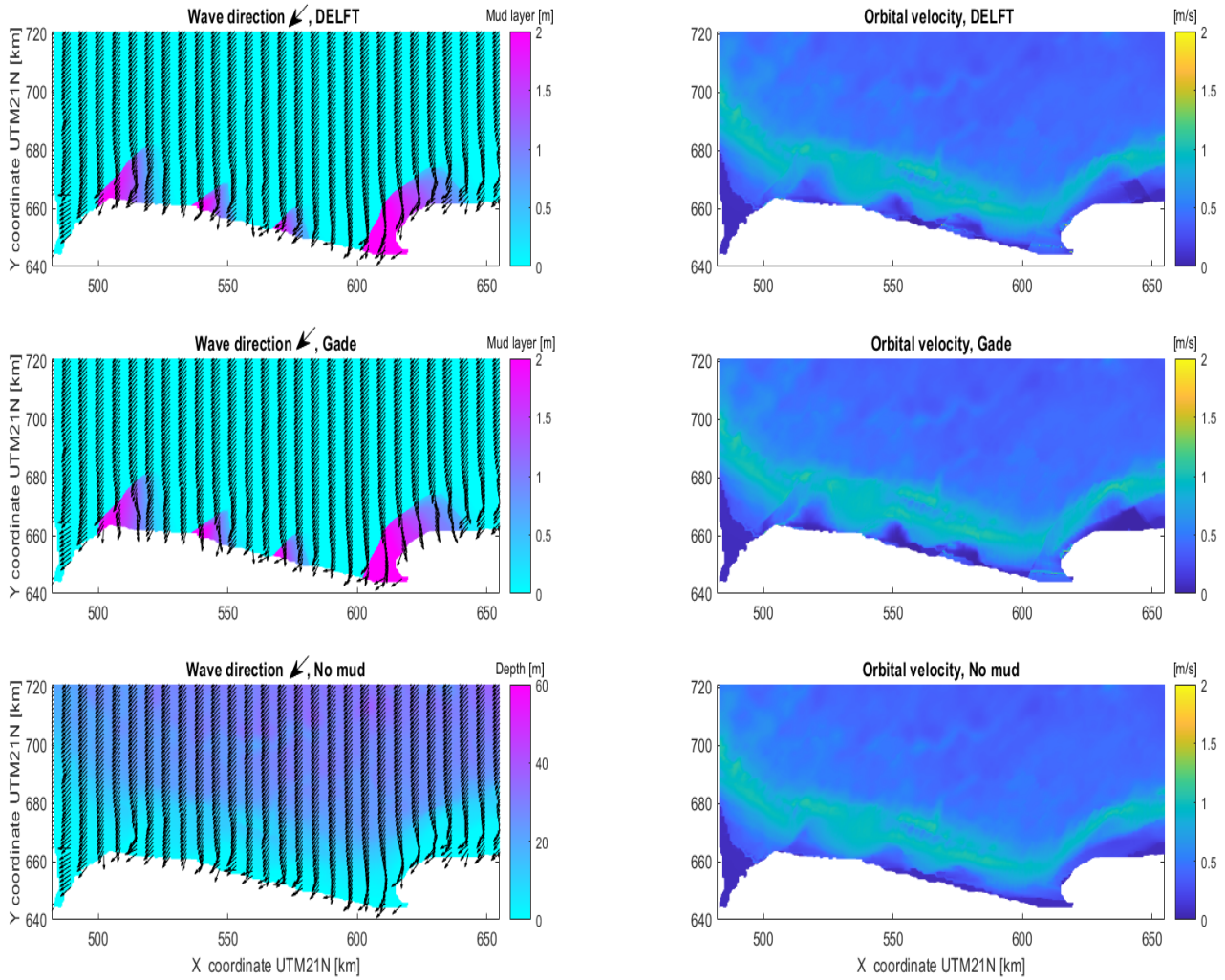

Figure 3.4: Spatial plots for wave direction indicated by arrows, 1st column, on top of the mud layer thickness in case of DELFT (1st row) and Gade (2nd row), and on top of the bathymetry for the case without mud (3rd row). Spatial plots of orbital velocity are presented in the right column using DELFT formulation (1st row), Gade (2nd row), and in the case without mud (3rd row).

is larger compared to DELFT. Very close to the shore, almost all of the energy in case of Gade is dissipated. However, there is a small peak in waves with periods of approximately 10 s, as indicated in Figure 3.4. In case of DELFT there is a pronounced shift of wave energy towards larger frequencies. This is explained by the dissipation of waves due to wave breaking and due to the mud layer. In the case without mud, there are two peaks in spectral density. There is a shift towards larger frequencies, where most of the energy is contained. This shift is associated with the energy transfer by the wind.

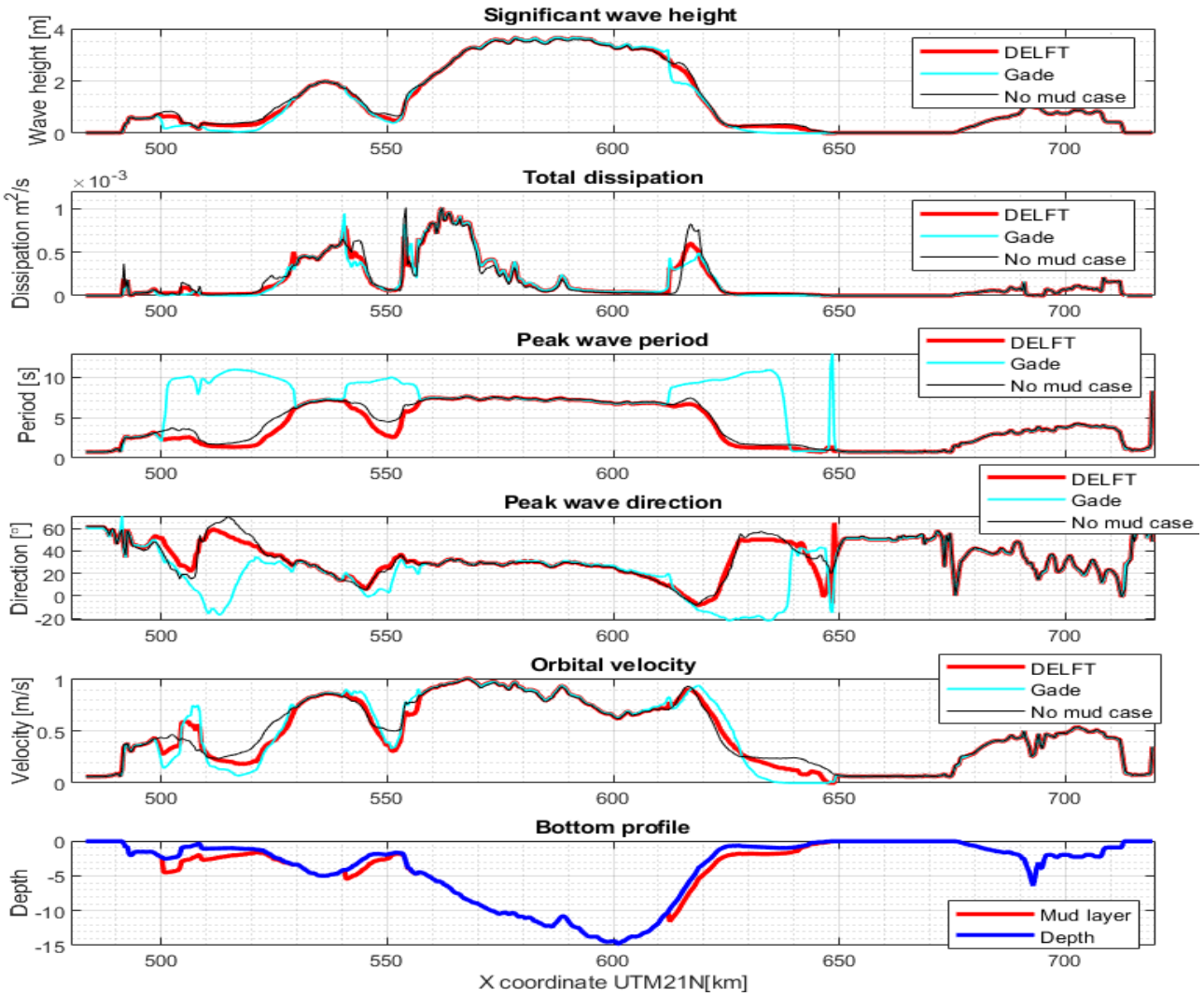

Figure 3.5: Alongshore section for the bathymetry indicated in Figure 2.3. The lower plot shows the water depth profile (blue line) and the mud patches (red lines). From top to bottom, the first plot shows the significant wave [m], the second total dissipation [m^2/s], the third peak wave period [s], the fourth peak wave direction [°] and the fifth orbital velocity [m/s]. The red line indicates DELFT formulation, the cyan line Gade formulation and the black line the case without mud.

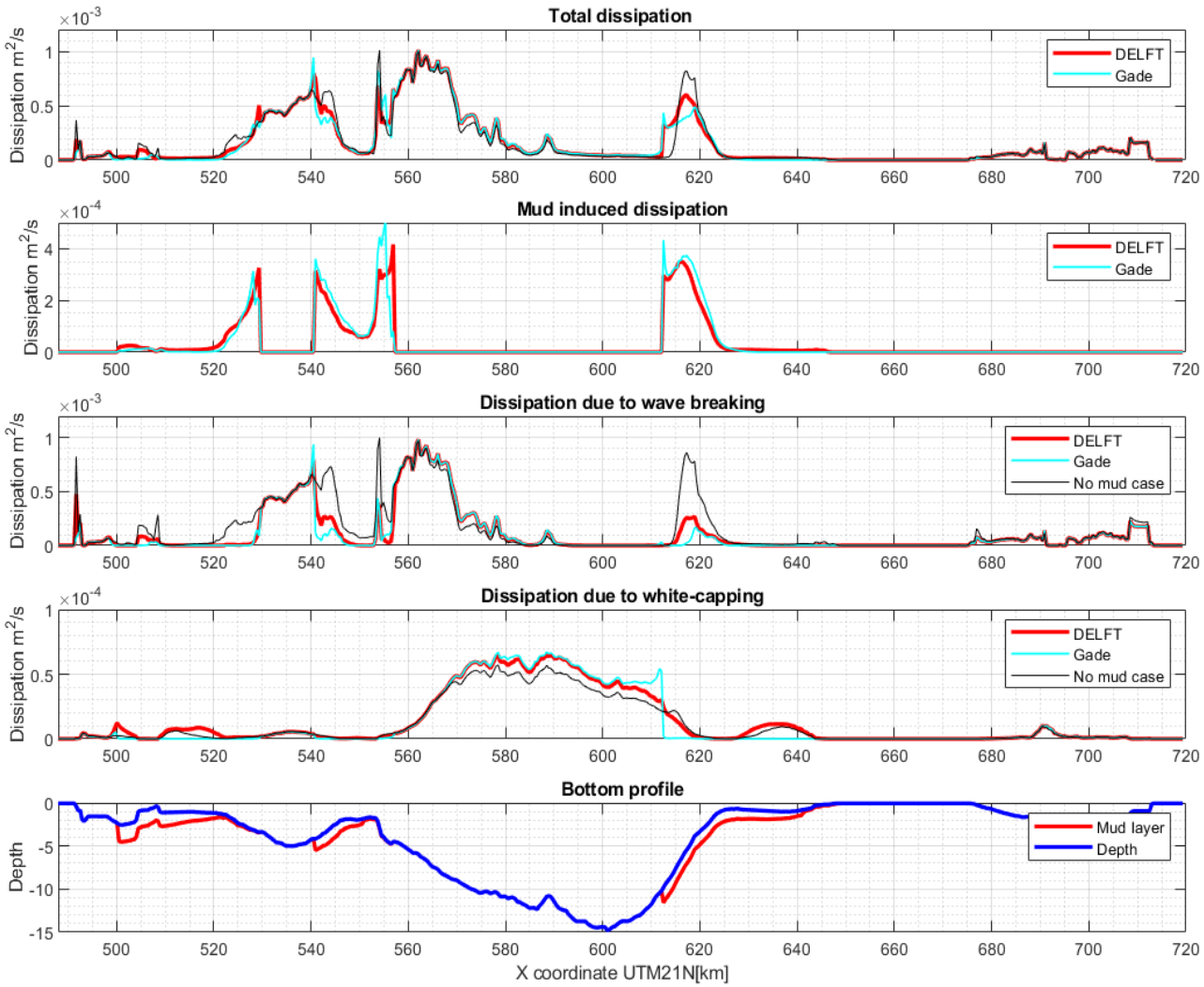

Figure 3.6: Alongshore section for the bathymetry indicated in Figure 2.3. The lower plot shows the water depth profile (blue line) and the mud patches (red lines). From top to bottom, the first plot shows total dissipation [m^2/s], the second mud induced dissipation [m^2/s], the third wave breaking induced dissipation [m^2/s] and the fourth dissipation from whitecapping [m^2/s]. The red line indicates DELFT formulation, the cyan line indicates Gade formulation and the black line the case without mud.

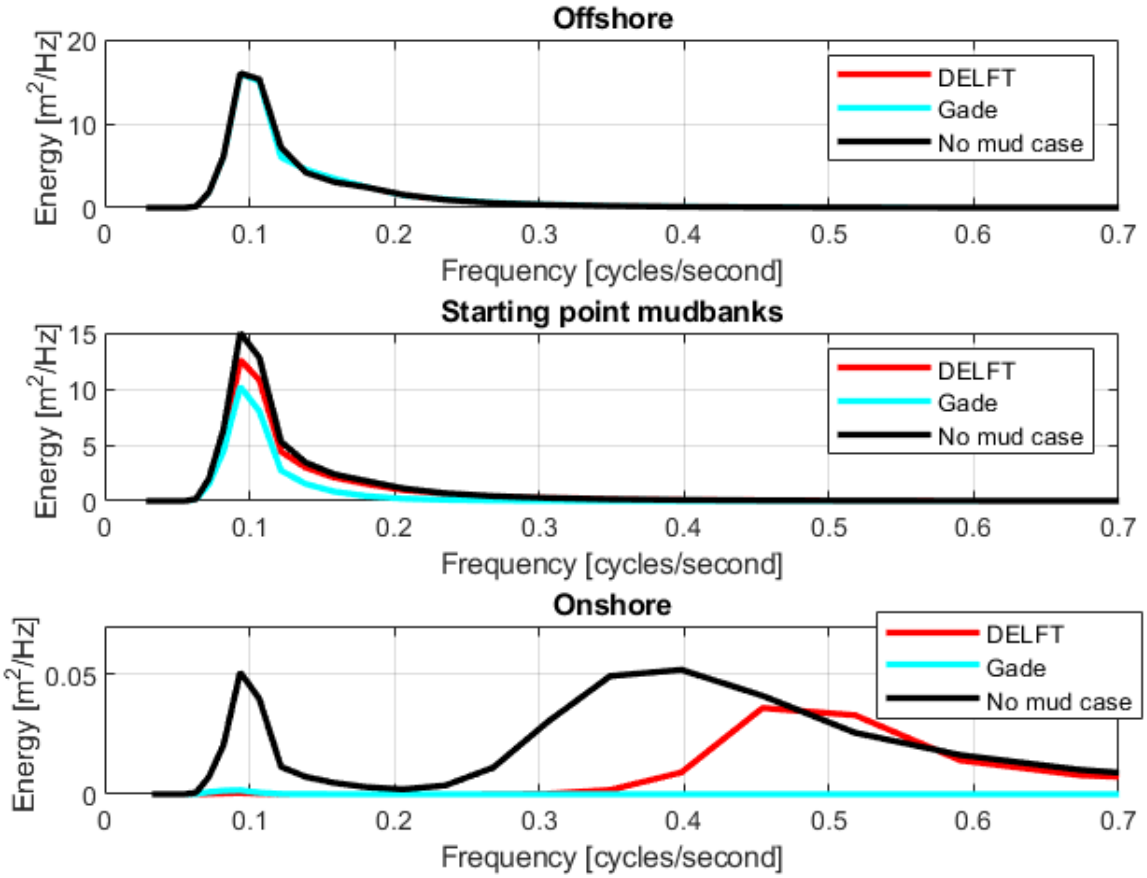

Figure 3.7: Wave spectra for three locations in the coast of Suriname. The red line indicates DELFT formulation, the cyan line Gade formulation and the black line the case without mud. The three locations where the wave spectrum is computed are indicated in Figure 2.3
. In the x-axis it is indicated the frequency in cycles per second or Hz and in the y-axis the wave energy in m^2/Hz. The y-axis has a different range in the three locations due to the different order of magnitudes of wave energy in each case.

3.1.2 Normal conditions

In the following section we look at a set of experiments with imposed normal boundary conditions, Section 2.2.3, Table 2.2. Spatial plots of significant wave height, wave period and total dissipation are given in Figure 3.8. An analysis of the same wave characteristics together with the wave period and the wave direction takes place along a cross-shore section in Figure 3.9. The dissipation sources are studied along the same cross-shore section in Figure 3.10. Spatial plots of wave direction and orbital velocity are given in Figure 3.11.

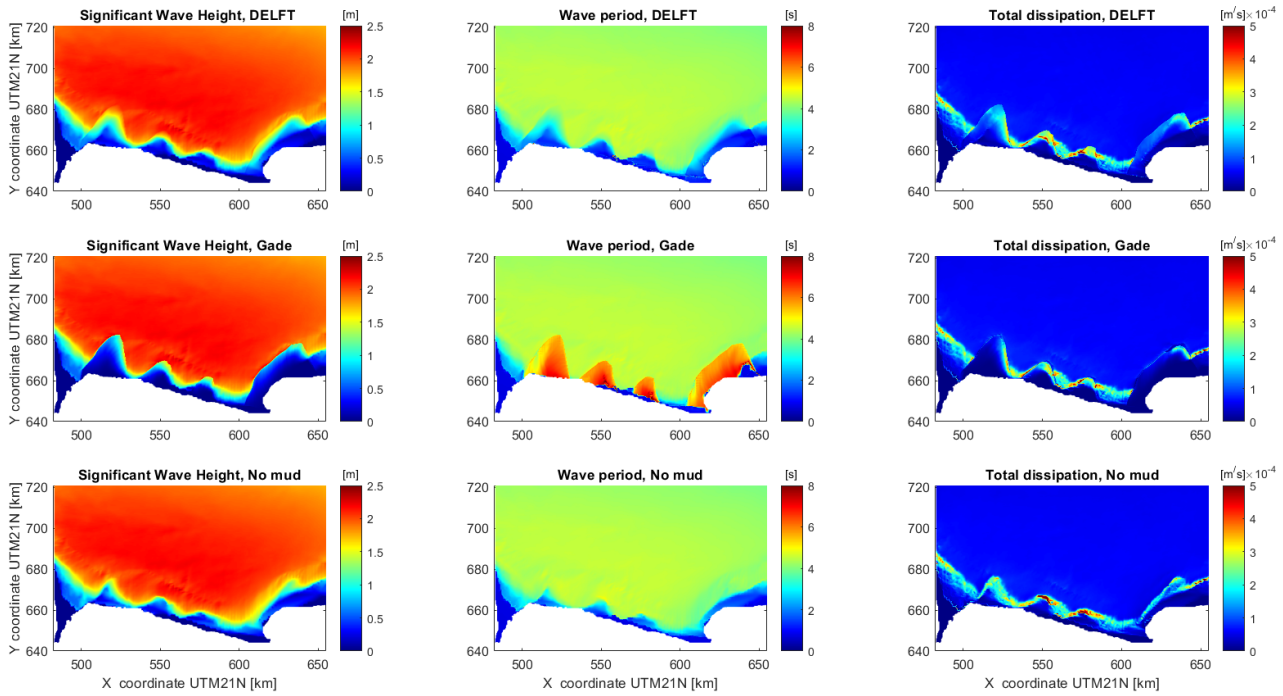

Figure 3.8: Plots for significant wave height [m] (1st column), wave period [s] (2nd column) and total dissipation [m^2/s] (3rd column). In the first row the results with DELFT formulation are presented (Kranenburg, 2011), in the second with Gade formulation (Gade, 1958) and in the last row the results for the case without mud are presented.

The pattern of the results is similar to the case with extreme conditions. In this case though, waves are purely wind generated. According to the spatial plots in Figure 3.8 and the cross-shore section in Figure 3.9 for normal conditions the fastest decrease in significant wave height is observed with Gade formulation, next with Delft and finally in the no mud case. The wave period in case of Gade, is significantly larger compared to the rest of the cases in the location of the mudbanks. In this case, when waves approach to the coast, the majority of the high frequency waves have dissipated and mainly the low frequency waves reach the coast Wells and Coleman (1981). The opposite pattern is observed in case of DELFT and in the no mud case. The wave dissipation is similar to the case of extreme conditions, in terms of mud induced dissipation, i.e. waves dissipate faster when they arrive at the location of the mudbanks. However, during extreme conditions there is more depth-induced wave breaking compared to normal conditions, simply because the waves are much higher in the first case. One major difference is that during normal conditions dissipation due to whitecapping is in the same order of magnitude compared to total dissipation. Moreover, during extreme conditions total dissipation in the offshore part is close to zero, however during normal conditions the total dissipation is of the same order of magnitude all over the domain. So whitecapping in this case is

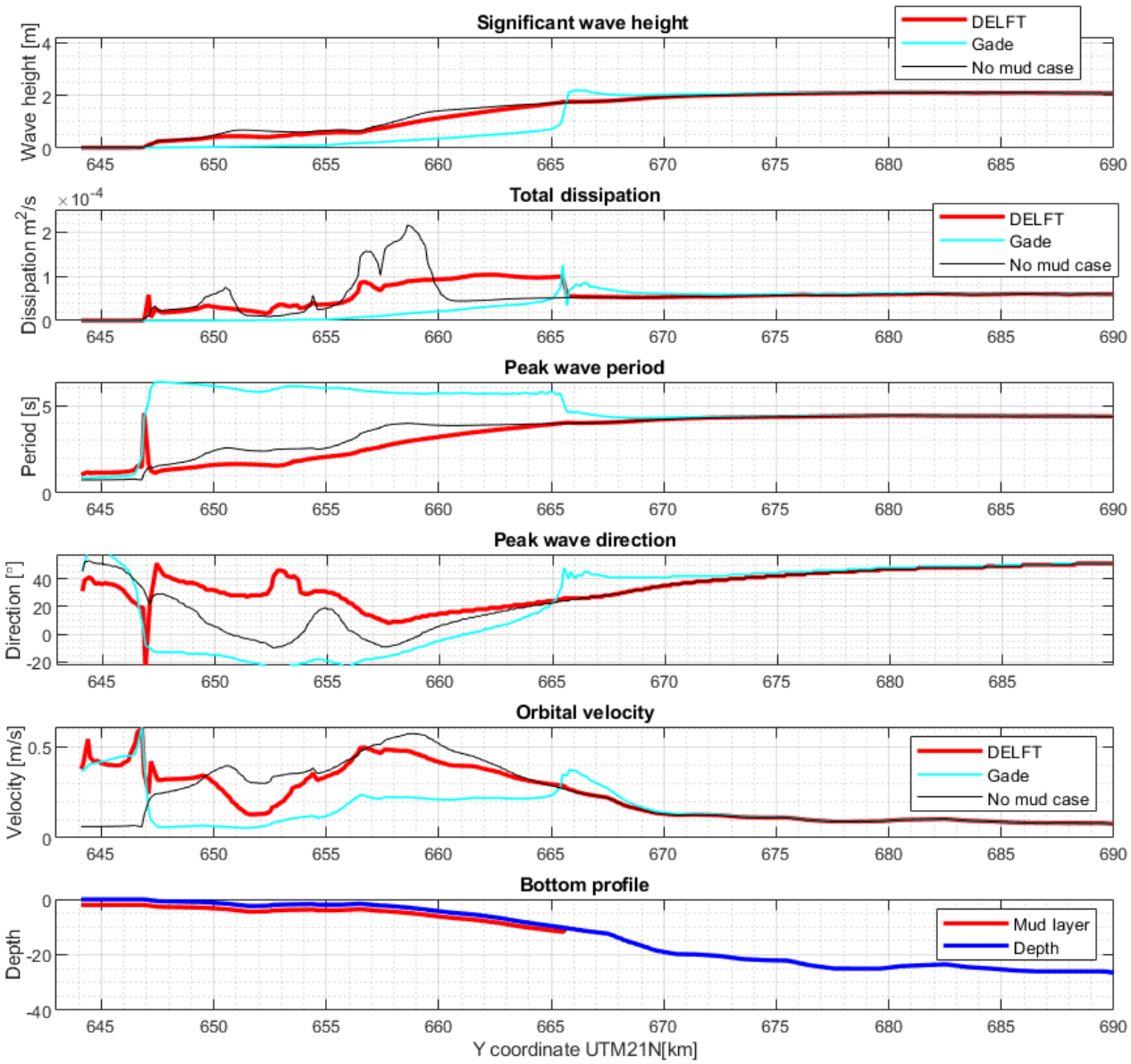

Figure 3.9: Cross-shore Section for the bathymetry indicated in Figure 2.3. The lower plot shows the water depth profile (blue line) and the mud patches (red lines). From top to bottom, the first plot shows the significant wave [m], the second total dissipation [m^2/s], the third peak wave period [s], the fourth peak wave direction [°] and the fifth orbital velocity [m/s]. The red line indicates DELFT formulation, the cyan line Gade formulation and the black line the case without mud.

significant (see Figure 3.10). Although the dissipation is significant in the offshore part, the reason for increase of wave height is the wind input.

The patterns in wave direction and orbital velocity are the similar as during extreme conditions. Wave direction changes significantly in the location of the mudbanks and especially in the case of Gade. The orbital velocity increases when waves propagate towards the shore and depth becomes smaller, and it decreases over the mud layer. A comparable shape is observed for the no mud case.

Again, orbital velocity is not zero at the coastline with DELFT and Gade formulations.

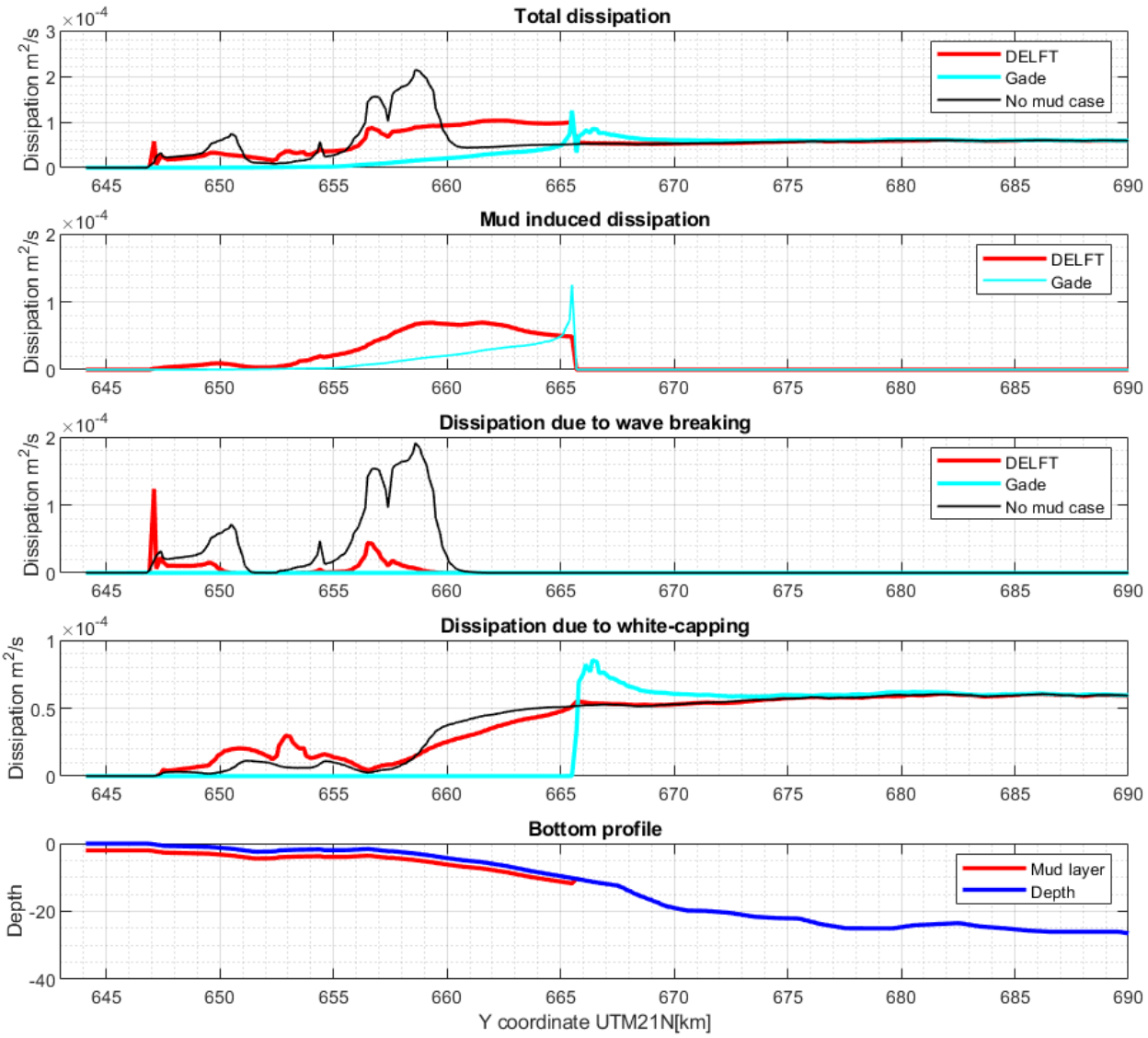

Figure 3.10: Cross-shore section for the bathymetry indicated in Figure 2.3. The lower plot shows the water depth profile (blue line) and the mud patches (red lines). From top to bottom, the first plot shows total dissipation m^2/s, the second mud induced dissipation m^2/s, the third wave breaking induced dissipation m^2/s and the fourth dissipation from whitecapping m^2/s. The red line indicates DELFT formulation, the cyan line Gade formulation and the black line the case without mud.

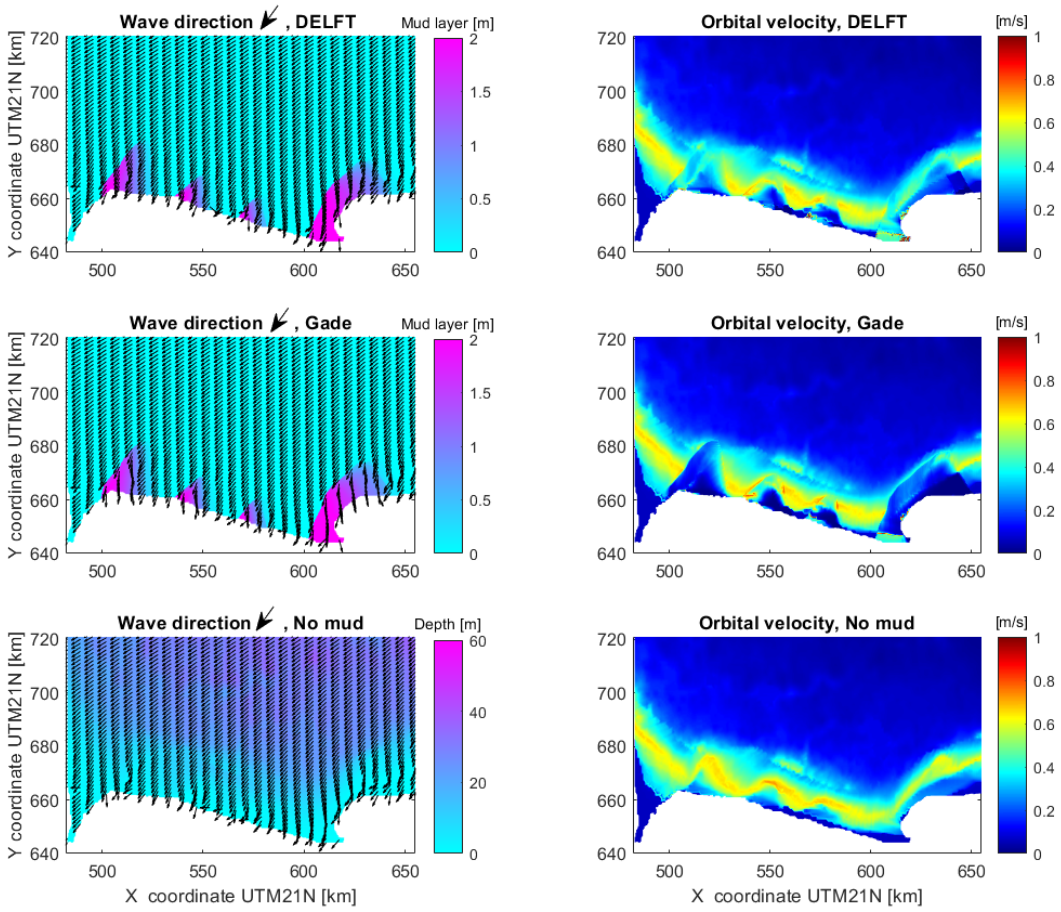

Figure 3.11: Spatial plots for wave direction indicated by arrows, 1st column, on top of the mud layer thickness in case of DELFT (1st row) and Gade (2nd row), and on top of the bathymetry for the case without mud (3rd row). Spatial plots of orbital velocity are presented in the right column using DELFT formulation (1st row), Gade (2nd row), and in the case without mud (3rd row).

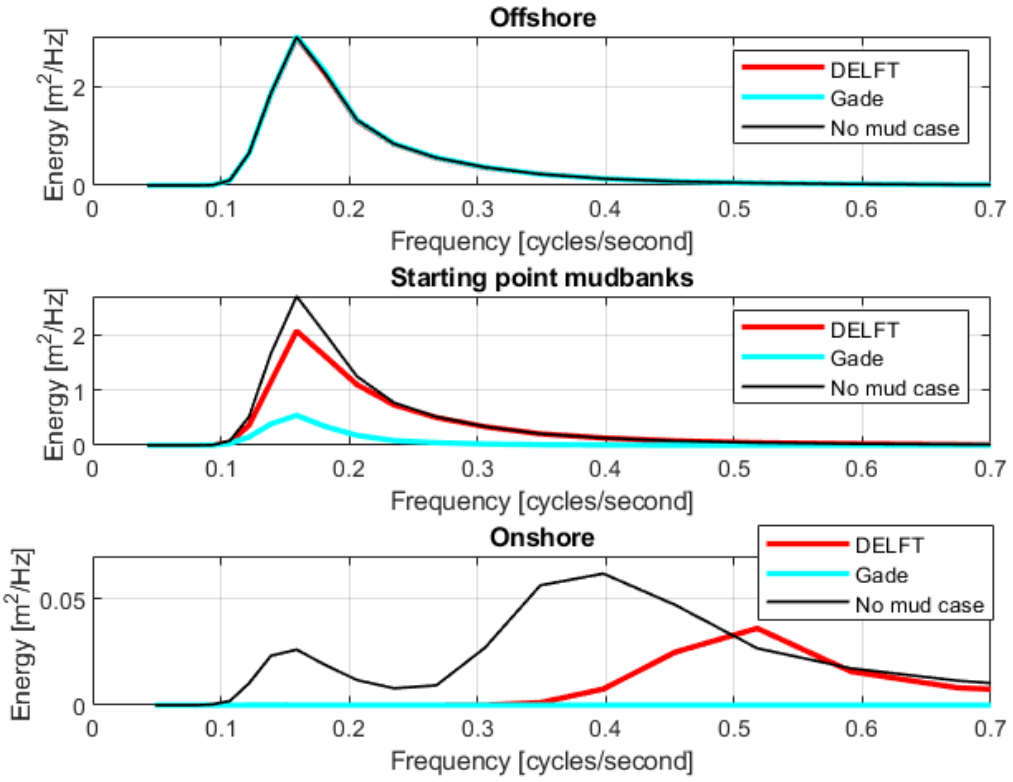

Figure 3.12: Wave spectra for three locations in the coast of Suriname in the case of normal conditions. The three locations are indicated in Figure 2.3. The red line indicates DELFT formulation, the cyan line Gade formulation and the black line the case without mud. In the x-axis it is indicated the frequency in cycles per second or Hz and in the y-axis the wave energy in m^2/Hz. The y-axis has a different range in the three locations due to the different order of magnitudes of wave energy in each case.

Figure 3.12 shows the wave spectra in the three locations indicated in Figure 2.3. In the offshore part, waves attain the same amount of energy in all three cases. All of the energy is found around frequencies of 0.15 Hz. In the case without mud, waves contain the most energy compared to waves with DELFT and Gade formulation. Mud-induced dissipation is again the reason why waves with DELFT and Gade formulation are more severely dissipated. Waves with Gade formulation contain the least energy, as there is a larger peak in wave dissipation compared to DELFT at the beginning of the mud layer. Finally, when waves have propagated over the mud layer, in case of Gade they have lost (almost) all of their energy. The last wave energy with DELFT formulation is contained in frequencies with 0.5 cycles/second. Most of the energy in the case without mud is found around frequencies of 0.4 cycles/second, while there is still some energy in the initial frequency.

3.2 Experiments with Delft3D

The first way to analyze the results from Delft3D-FLOW is to compare the output data of water level with the observations from the local tidal station, Surinamentriho (red asterisk) in Figure 2.2. The RMSE error according to Equation 2.36 in this case is 0.1662 m. In order to further investigate if the simulation is stable and the flow is undisturbed in the boundaries, the depth averaged velocity direction is plotted on top of the water level for chosen time points. Results can be seen in Figure 3.13. The flow is indeed undisturbed and the simulation is valid.

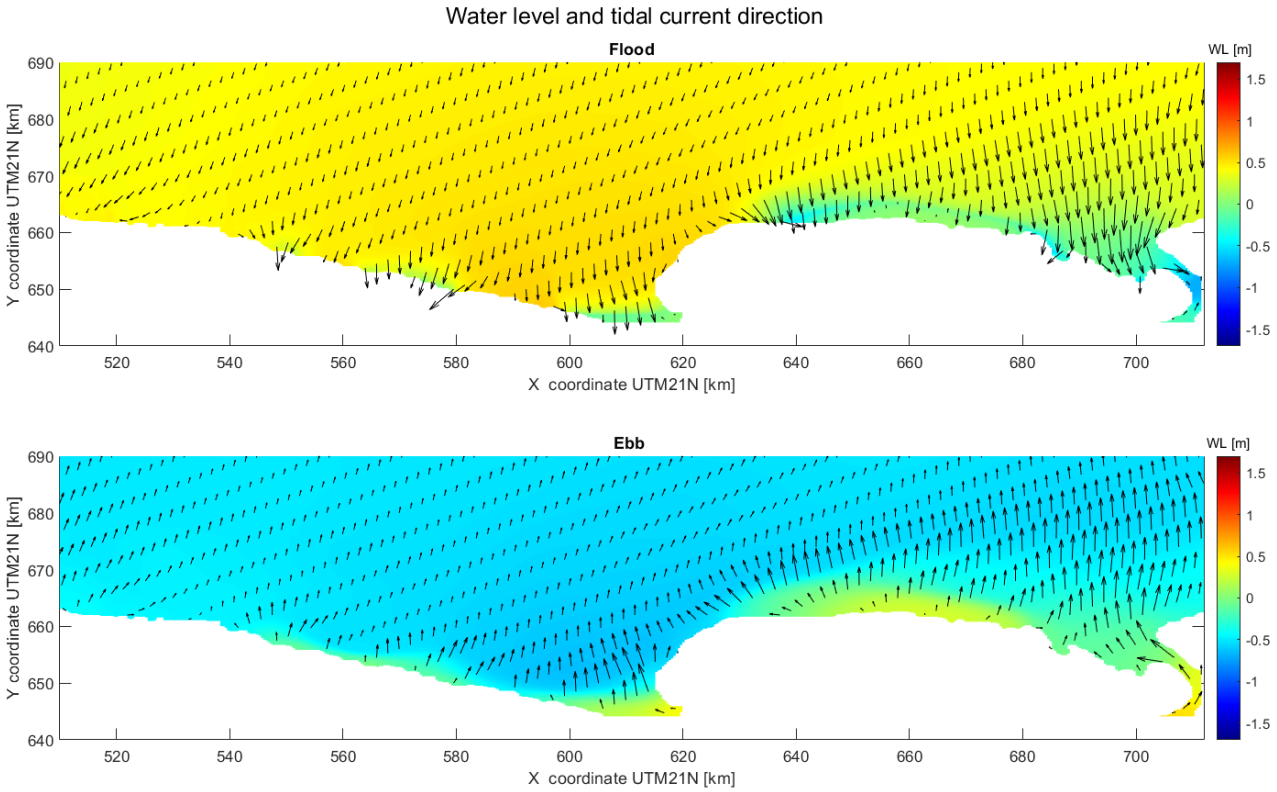

Figure 3.13: The water level (colour contours, in m) and depth averaged velocity direction (arrows) are shown for flood (top plot) and ebb (bottom plot). The length of the arrows show the magnitude of the depth averaged velocity. The maximum value it attains is approximately 1 m/s. The time difference between the two cases is 12 hours.

First, a harmonic analysis is applied in the water level as described in Section 2.3. According to Nedeco (1968); Wells and Coleman (1981) the tides in the coast of Suriname are mainly semi-diurnal. The amplitude for the tidal constituents M2, M4, S2 and K1 are shown in Figure 3.14. Indeed the results from the harmonic analysis indicate that M2 has the largest amplitude and so M2 is the most dominant tidal constituent. However, water level amplitude is expected to increase eastwards, according to Figure 3 of Kagan and Sofina (2014). In Figure 3.14, this is not the case, as there is no clear pattern of an increase in west-east direction for all constituents.

Since M2 is the most dominant tidal constituent, its phase is also discussed. A plot with iso-phase lines is provided in Figure 3.15 for the small, physical domain. The phase of M2 is expected to be uniform along the coast of Suriname according to Kagan and Sofina (2014), with changes only very close to the shore. Results from simulations with Delft3D-FLOW are in agreement with literature. Pronounced differences in tidal phase are usually associated with the local features of the bottom

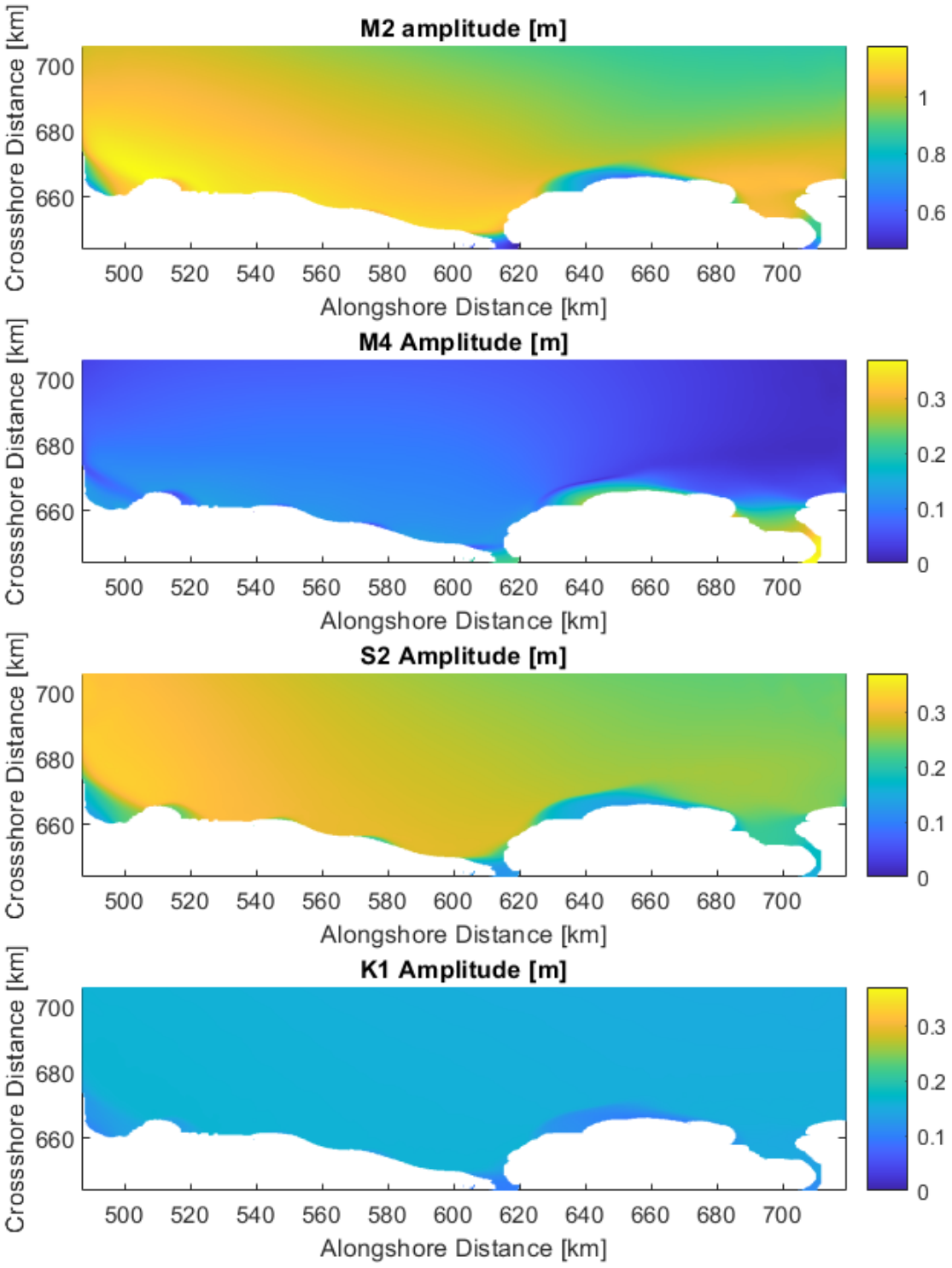

Figure 3.14: Tidal analysis: amplitude of tidal constituents M2, M4, S2 and K1.

topography, and they are observed very close to the shoreline (Pugh and Woodworth, 2014). A similar plot is provided for the overall domain in order to establish the correct pattern of M2 phase in Figure 3.16. Although the overall domain is of low accuracy (in order to facilitate fast numerical simulations) the results show the expected results, that there is not significant change in phase also in this case.

A harmonic analysis is also applied on the velocity components of the tidal current in order to

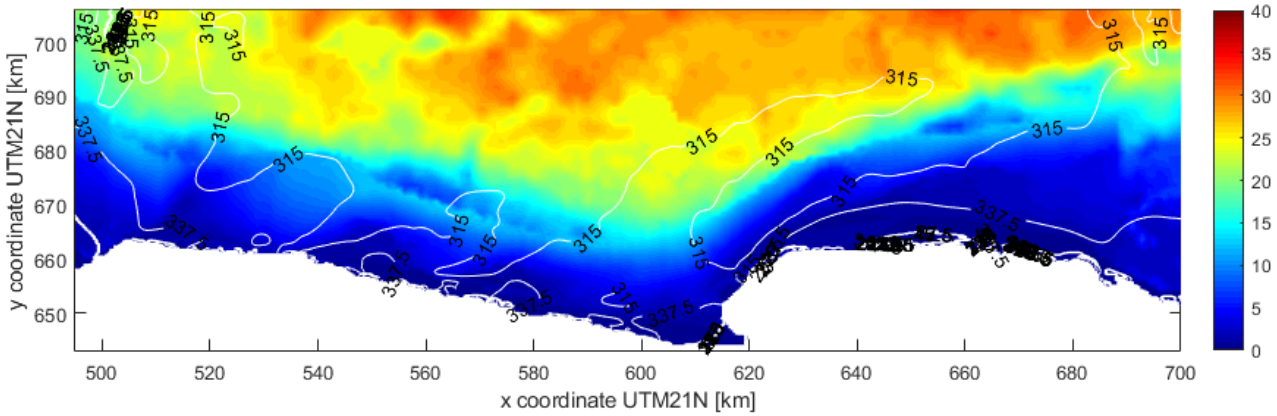

Figure 3.15: Plot of equal tidal phase lines (white lines) for the physical domain on top of bathymetry, colored in m. Numbers across the white lines indicate the tidal phase in degrees.

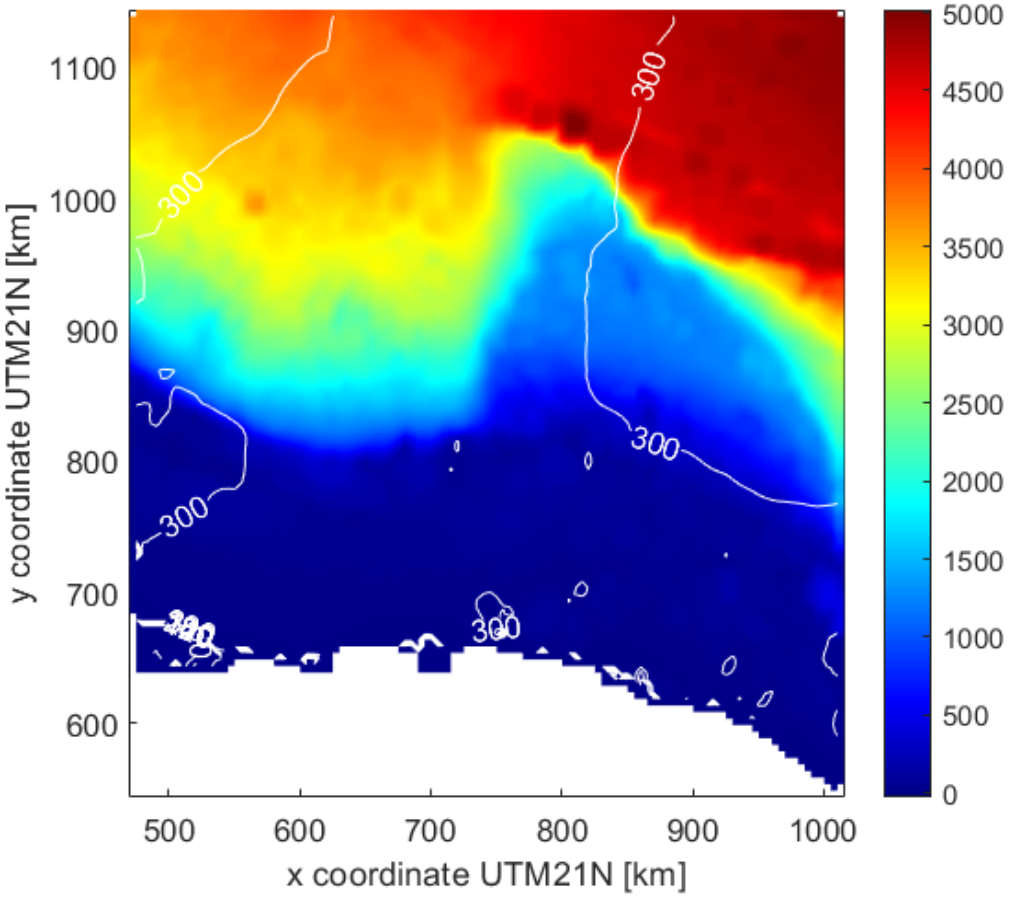

Figure 3.16: Plot of equal tidal phase lines (white lines) for the overall domain on top of bathymetry, colored in m. Numbers across the white lines indicate the tidal phase in degrees.

obtain the main direction of the tides along the coast of Suriname. Plots of tidal ellipses on top of the bathymetry show that tides are directed normal to the coast as shown in Figure 3.17. This is in accordance with the literature Augustinus (1978). In the same figure, it is observed that the tidal current rotates clockwise in the offshore part, and anticlockwise in the onshore part. The change in

direction could be associated with the increased friction in shallow waters.

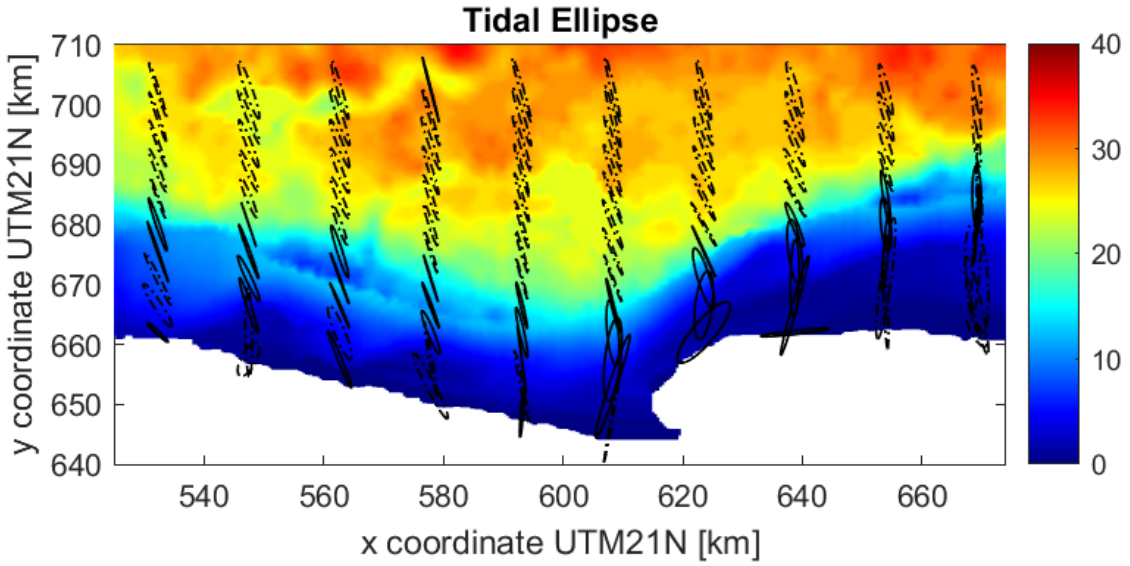

Figure 3.17: Plots of tidal ellipses and bathymetry colored in m.The tidal ellipse shows the main direction of the tidal current. The ellipses with solid lines indicate tidal currents that rotate anti-clockwise while ellipses with dashed lines indicate tidal currents that rotate clockwise.

Chapter 4

Discussion

In this chapter, the results of all the experiments that are presented in Chapter 3 are discussed. More particularly, in Section 4.1 the common limitations of the model-set up of the 2D experiments for SWAN-Mud and Delft3D are elaborated. The results from experiments aiming at reproducing earlier work are analyzed in Section 4.2, the results from experiments with SWAN-Mud in Section 4.3, the results from experiments with Delft3D in Section 4.4 and in the last Section 4.5, recommendations are given for future research.

4.1 Model assumptions

Many assumptions are made in Section 2.2, where the model set-up of the experiments is discussed. These assumptions are categorized in three groups: assumptions regarding the bathymetry, the mud properties and assumptions regarding the physical processes that are studied.

The stronger constraint throughout this study is the lack of data availability that inevitably led to many simplifications during the simulations. One of these constraints has to do with the bathymetry that was used. First of all we assume the bathymetry to be fixed during simulations, while actually especially in the nearshore zone the bottom topography is highly dynamic. This is because of the fluidization and mobilization of the upper fluid mud layer that affect the bathymetry. There is only one reliable bathymetry from 2016, that was combined with the bathymetry from GEBCO (GEBCO) dataset, under the assumption that no significant changes in the offshore bottom topography between the two dates for each case take place. The order of magnitude of the changes ranges up to a few meters, but in any case offshore changes in bottom topography are not per se relevant. However, the accuracy of the nearshore bathymetry is not a priority since it has been established that the main calibration parameter, when studying muddy environments similar to the one in Suriname, is the mud viscosity (Winterwerp, 2007).

As a result, the values for the mud properties, viscosity and density, are taken from the final results of Winterwerp (2007) where the coast of Guyana is studied. As already mentioned, the design of the thickness of the mudbanks takes place according to a literature review (Augustinus, 1978; Wells and Coleman, 1981; Anthony et al., 2008; Toorman et al., 2018), discussion with experts on the field, and according to the bathymetry data (the thick patches that are obvious in bathymetry). Also, the mud density and viscosity are uniform all over the domain under the assumption that differences along the coastline are negligible and because there is one large sediment input, Amazon's outflow. However, there is a high degree of uncertainty here, since there are not recent direct measurements. The mud viscosity together with mud thickness are of high importance in the dissipation of waves. These properties are not expected to vary significantly over time. However, they might vary on the scale of one mudbank, as mud density and viscosity are expected to increase from east to west, as a

result of the mud thickness increase in same pattern. The latter, represents an assumption and needs to be further investigate

In the end, the assumptions that have to do with the physical processes are analyzed. In all simulations the wind input is constant over the domain. However, during extreme (storm) conditions the wind magnitude and direction vary. Moreover, the see breeze modulation during normal conditions is also important. However, the constant wind input from the trade winds is the largest and does not change significantly. As a consequence, it should be further studied whether differences in the wind input play a critical role on wave dissipation and tidal current propagation. It is also important to note that the effects of baroclinicity are not taken into account. Baroclinicity effects are related with the fresh water input of Amazon and the high stratification that is present. There is also uncertainty regarding the coastline of Suriname. The design of the computational grids took place according to the latest landboundaries available in Delft-Dashboard and according to the available bathymetry. Finally, the mangrove forests are not implemented in the model set-up and as a result they are not taken into account into the wave dissipation. Mangroves are found usually at the mean high tide level Toorman et al. (2018). When mangroves are included in the model, wave dissipation is expected to be larger but at the scale of a few meters to 100 meters. Consequently, the wave dissipation due to the mangroves should be quantified, in order to determine how critical the role of the mangroves is in preventing coastal erosion.

4.2 Reprodicibility of results of earlier studies

During the experiments on reproduction of earlier work that are described in Appendix A, some assumptions were made as well. The 1D experiment that aims at reproducing the laboratory data from De Wit (1995) is in full agreement with the original data, and both DELFT and Gade formulations are able to give reliable results. The experiment in Guyana from Winterwerp (2007) also shows that SWAN-Mud is able to reproduce large scale 2D experiments. The results with DELFT formulation are in accordance with the results in the related experiment as the obtained patterns in significant wave height, wave dissipation, wave period and wave energy follow similar patterns to the ones of Suriname. It should be noted though, that in the latter case the design of the mudbanks varies significantly. More particular, the mudbanks in Suriname extend up to 15 km offshore (not up to 30 km), they are smaller in thickness and their thickness varies in the zonal direction and not in the meridional as in Winterwerp (2007). Results with Gade formulation show a different pattern in wave energy distribution compared to DELFT formulation, i.e. near the coast there are almost only low-frequency waves. There results are in agreement with field observation from Wells and Coleman (1981) (Appendix A). This result is of major importance as it has been established that Gade formulation is not suitable for muddy environments as the one in Suriname or Guyana, however field observations validate these results. Finally, numerical issues were encountered when the 1D experiments from Figure 7, Kranenburg (2011) and Figure 3.4.5, De Wit (1995) were repeated (see section A.2). It was not possible to obtain an optimum mud layer thickness with DELFT formulation, but only with Gade formulation. This suggests the possibility of technical issues in SWAN-Mud (see Section A.2.4). Knowledge of this parameter can prove useful in case measures are taken for protecting the coast. Although the coastal area is highly dynamic, a mud layer of the optimum mud thickness could be effective in dissipating waves.

4.3 Experiments with SWAN-Mud for the case in Suriname coast

As already discussed in Section 4.1, the lack of wave data availability makes it possible to compare the case in Suriname only with previous studies in literature. More particular, the wave dissipation is compared to the results from Winterwerp (2007); Wells and Coleman (1981). Two formulations are studied: DELFT formulation (Kranenburg, 2011), which is applicable in Suriname and it is considered the reference case, and Gade formulation (Gade, 1958) that might not be applicable to Suriname according to the theory (shallow water limitation, see Section 2.1.1.3) but it is in agreement with field measurements in Suriname by Wells and Coleman (1981).

More particular, results with DELFT parameterization are in full agreement with the results in Winterwerp (2007). Although there are no direct measurements in order to validate the model outputs, the results with this formulation show similar patterns for the main wave characteristics, i.e. as soon as waves meet the mud layer the significant wave height reduces, wave dissipation increases and wave period decreases. In case of Gade though, the distribution of the wave energy is in agreement with Wells and Coleman (1981), i.e. only low frequency waves arrive to the coast (opposite in DELFT). So, although this formulation is not fully applicable in the coast of Suriname, reliable results can be derived that are in line with findings from literature. Although the results from both formulations are in accordance with studies in the literature, it can be concluded that there is a strong difference between them, i.e. in the wave energy distribution.

Consequently, in order to improve the answer to the first research question, i.e. if SWAN-Mud can simulate wave characteristics, a more detailed analysis is needed. This means, a more accurate bottom and mud topography, measurements of mud density and viscosity and application of non-uniform layers of these two variables. Wind plays an important role in this area, so a varying wind is necessary as well for more accurate simulations. In the end, wave data are of highest importance in order to validate the model and derive robust results.

4.4 Experiments with Delft3D

The availability of astronomical tidal boundary conditions makes the results from Delft3D-FLOW reliable. Although the RMSE between the modelled water level elevations and observations is 0.1662 m, and the water level amplitude pattern of M2 is not in full agreement with values in literature, the large scale tidal properties are representative. M2 is the most dominant tidal constituent Augustinus (1978), M2 phase does not very significantly, and the tidal currents arrive normal to the coast (see Section 3.2).

Coupling between Delft3D-FLOW and Delft3D-WAVE does not take place because Delft3D-WAVE uses the regular version of SWAN, that does cannot account for the mud layer. However, efforts took place throughout this study so that a successful coupling between SWAN-Mud and Delft3D-WAVE is done (as a first step before Delft3D-WAVE with SWAN-MUD is coupled to Delft3D-FLOW). So far, these efforts have not resulted in a successful coupling between these models. For future, morphodynamic studies, the results can be significantly improved in case it is possible to conduct coupled experiments between Delft3D-FLOW and the state of the art numerical wave model SWAN-Mud.

4.5 Recommendations for further research

Suggested improvements for SWAN-Mud:

- The most important step that needs to be made in order to successfully use SWAN-Mud v40.61 (used in this study) in the future is to compile the source code, and check whether all formulations work as suggested in the manual (description of related problems can be found in Section A.1 and a detailed analysis of the problems in Section A.2.4). In order to validate the model simple 1D tests are capable of distinguishing between the different formulations (such tests are described in Kranenburg (2011), Figure 2 and Figure 7).

- If possible, it should be studied why De Wit formulation does not take into account the mud layer (description of related problems can be found in Appendix A.1 and why Ng formulation gives only NaNs in case of large scale 2D experiments. The latest version of SWAN-Mud includes a more advanced version of Ng formulation that is supposed to be more advanced than the DELFT dispersion relation.

- Besides validating that the formulations that are included in the model work as expected, it is also important to validate the model with field observations. Mud viscosity is one of the most important factors to influence wave dissipation (Winterwerp, 2007). As a result, field measurements of the mud properties are necessary. Accurate observations of the bottom topography and of the mud layer thickness can contribute in simulating the coastal area of Suriname in a larger degree of accuracy. Finally sufficient timeseries of wave data are crucial in order to establish the validity of the model.

- In order to further improve the accuracy of the model it is important not to neglect physical processes that are of major importance in the coastal area of Suriname. This could be a varying wind input, the the observed stratification (baroclinicity effects), the mangrove induced wave dissipation.

Next steps for coupling Delft3D-Flow and SWAN-Mud:

- The first step in order to couple SWAN-Mud with Delft3D-WAVE is to take into account that SWAN-Mud requires more inputs compared to the regular version of SWAN, that have to do with the input parameters of mud properties. These parameters are the mud layer thickness, the mud density and viscosity, the water density, and inputs that indicate which formulation is used. It should be noted that these parameters are necessary in order SWAN-Mud runs. This is a strong compatibility problem between Delft3D-WAVE and SWAN-Mud, as Delft3D-WAVE cannot ”recognise” these parameters. The possible solution to this problem is the edit of the batch files with which Delft3D-WAVE and SWAN (any version of SWAN) communicate. This compatibility problem is bypassed during this study, however more problems occured.

- Even if SWAN-MUD is able to successfully ”communicate” with Delft3D-WAVE, the main constraint that hinders the coupling is that the outputs of Delft3D-WAVE contain errors as they are not designed to give outputs of parameters that depend on the mud layer (e.g. mud induced dissipation).

- In case a successful coupling between Delft3D-WAVE and SWAN-MUD takes place, it is not certain if Delft3D-WAVE will be successfully coupled to Delft3D-FLOW for the case of online-coupling, i.e. bed level updates.

- It is also important to note that the latest SWAN version v41.31 can be activated in order to account for muddy environments. In this version, Ng formulation (Ng, 2000) is implemented. However, testing of this version indicates that large scale 2D experiments are also not possible as results contain NaN values (Not a Number values). It is recommended that more experiments with this version take place.

Chapter 5

Conclusions

This study is presenting for the first time spatial information of wave characteristics in the complex coastal area of Suriname. More particularly, it aims at identifying whether the two numerical models SWAN-Mud and Delft3D are able to successfully simulate waves and currents in muddy coastal environments like the one in Suriname. Answers to the first and the second research questions are found in Sections 5.1 and 5.2 respectively.

5.1 First research question

In order to answer the first research question, i.e. if SWAN-Mud can successfully simulate waves at the coast of Suriname, experiments take place with two formulations, DELFT and Gade. Results with DELFT formulation are in accordance with Winterwerp (2007) and results with Gade formulation are in accordance with Wells and Coleman (1981) (see Section 3.1. However, there is a significant difference in the results regarding the wave energy distribution. In the first case the peak wave energy is shifted towards higher frequencies, while in the second, the peak wave energy is shifted towards lower frequencies compared to the initial frequency with which waves were forced. Consequently, results from SWAN-Mud can be explained by studies in literature, although these results are contradicting. So, it needs to be further investigated which of the two cases is the most realistic.

Taking into account the above-mentioned results and all the assumptions that were used for these simulations, we can conclude that SWAN-Mud can be used for future simulations in muddy coastal environments as it can simulate successfully wave characteristics like the significant wave height, wave dissipation, wave direction and near bed orbital velocity.

5.2 Second research question

The second research question tests the applicability of Delft3D-Flow to study the hydrodynamics in muddy environments, like the one in Suriname. The comparison between water level observations and model outputs does not give a small RMSE value and the amplitude of the water level is not in full accordance with results in literature (Kagan and Sofina, 2014). However, the strong dominance of M2 tidal constituent on water levels, its phase pattern and the larger scale tidal characteristics, like the tidal current propagation direction are in agreement with previous findings (Augustinus, 1978). The direction of the tidal current is perpendicular to the coast, and the tidal phase does not vary in the broader coastal area of Suriname. As a result, it can be concluded that Delft3D-FLOW is a reliable numerical model for future studies in muddy environments like the one in Suriname.

Finally, coupling between Delft3D-FLOW and Delft3D-WAVE does not take place, as the latter

uses the regular version of SWAN that cannot take into account the mud layer. Results from Delft3D are expected to be of higher accuracy if it is coupled to SWAN-Mud. In this case, it will be possible to use it for high-resolution morphodynamic studies and accurately model erosion, transport, and deposition of mud.

Appendix A

Appendix

A.1 Reproduction of earlier work

De Wit (1995) first conducted a laboratory experiment where he studied waves propagating over a mud layer and tested the wave attenuation rate. After the laboratory experiment he repeated the same case mathematically, soon after improving and extending the analytical model Gade (1958) developed. The set of equations he used are explained in De Wit (1995) and are also used in Winterwerp (2007). The latter, repeated the same 1D experiment and also performed some new 2D experiments for the coastline of Guyana (section 1.3). Both of these cases are performed in the current study, however using a newer version of SWAN-Mud, v40.61.

In the first case all necessary inputs are available in order to repeat the 1D experiment. For this case, a simple 1D grid of length 8 m is needed. The input parameters are listed in Table A.1. The experiment is conducted using the formulation of Gade (1958) and Kranenburg (2011). The formulation from De Wit (1995) will not be analyzed in this experiment. The reason is errors that arise during 2D simulations with this parameterization and lead to the conclusion that this parameterization does not give valid results with SWAN-Mud. This conclusion will be established later.

Significant wave height H_s	0.045 m
Water depth h_w	0.325 m
Domain length	8 m
Mud thickness h_m	0.115 m
Period	1.5 s
Mud viscosity	0.026 m^2/s
Mud Density	1300 kg/m^3
Water Density	1000 kg/m^3

Table A.1: 1D experiment on wave dissipation by fluid mud (De Wit, 1995), (Winterwerp, 2007).

In the second case (Guyana coastline), the bathymetry and the mud layer thickness are not directly available. The bathymetry is obtained from the GEBCO bathymetry dataset, and the mud layer thickness is designed with the same tools that were used in section 2.2.2. The mud layer thickness is designed according to Figure 10 from (Winterwerp, 2007) and most of the input parameters are obtained from the same paper. The goal of this experiment is to observe approximately the same behaviour of the most significant wave properties, i.e. significant wave height, wave period and dissipation of waves. The mud layer in this case is not similar to what is described in papers from Augustinus (1980), Wells and Coleman (1981), Froidefond et al. (1988). Namely the mudbanks in Figure A.2b are not triangularly shaped, with a steep slope from the east to west, and they are not

directly attached to the shoreline. There is not an indication of the trailing (erosional) or of the leading (depositional) edge. Instead they are more uniform, and their thickness decreases closer to the shore. However, this paper is one of the few that discusses numerical outputs for simulations that take place close to the Suriname coast. The input parameters are presented in the Table A.2. The experiment is conducted using the formulation of Gade (1958) and Kranenburg (2011).

Parameter	Description	Value
H_s	Forcing significant Wave Height	4 m
T	Period significant Wave Height	10 s
Dir H_s	Direction significant wave height	45°
DD	Directional spreading significant wave height	25°
	Boundaries for forcing H_s	North, East
W_s	Wind speed	12.5 m/s
Dir W_s	Direction wind speed	45 °
h_m	Mud viscosity	0.001 m^2/s
ρ_m	Mud density	1400 kg/m^3
ρ_w	1000 kg/m^3	1000 kg/m^3

Table A.2: Input parameters for 2D experiment in Guyana (Winterwerp, 2007)

Most of the input parameters for the case in Guyana are identical to the ones in the case which is studied in Suriname. As already explained, this happens due to the lack of data regarding the mud properties and under the assumption that the mud properties and the wave conditions do not change significantly between the two locations. Here, the formulations of Gade and DELFT will be compared with the original outputs from Winterwerp (2007).

The last experiments that aim at reproducing the results from previous studies target the computation of the mud layer thickness that induces maximum wave attenuation (parameter k_i). For this, simple 1D experiments from Kranenburg (2011) and De Wit (1995) are performed, the ones described in the Figure 7 and Figure 3.4.5 from the corresponding papers respectively. The model setup for these cases is given in Table A.3. Together with these experiments the optimum mud layer thickness for maximum wave attenuation is calculated for the case in Suriname. The input parameters for this experiment are given in the same Table. The results are presented schematically. To facilitate comparison it is suggested to perform normalization (Gade, 1958; De Wit, 1995; Kranenburg, 2011). The wave number (its real and imaginary part) is normalized with the wave number k for situations without (fluid) mud and the mud layer thickness is normalized with the Stokes viscous boundary layer $\delta_{BL} = \sqrt{\frac{2\nu_m}{\sigma}}$.

Parameter	Kranenburg (2008)	De Wit (1995)	Suriname 2020
Significant wave height H_s	0.5 m	0.5 m	0.5 m
Water depth h_w	4 m	1.5 m	4 m
Domain length	4000 m	500 m	4000 m
Mud thickness h_m	variable	variable	variable
Mud viscosity	0.5 m^2/s	0.1 m^2/s	0.001 m^2/s
Mud Density	1750 kg/m^3	1500 kg/m^3	1750 kg/m^3
Water Density	1000 kg/m^3	1000 kg/m^3	1000 kg/m^3

Table A.3: 1D experiment on wave dissipation by fluid mud (De Wit, 1995), Winterwerp (2007), Suriname.

In Table A.4 a list of the experiments that aim at reproducing the results of previous studies is presented.

Experiments on reproduction of earlier work		
Experiment No.	Description	Details
Experiment 1	1D laboratory case: Damping rate of waves that propagate over a mud layer (De Wit, 1995; Winterwerp, 2007)	Table A.1
Experiment 2	2D case Guyana: effect of the mudbanks on waves (Winterwerp, 2007)	Table A.2
Experiment 3	Mud layer thickness for maximum wave attenuation, Figure 7 (Kranenburg, 2011)	Table A.3
Experiment 4	Mud layer thickness for maximum wave attenuation, Figure 3.4.5 (De Wit, 1995)	Table A.3

Table A.4: List of experiments on reproduction of earlier work (Experiments 1, 2, 3, 4) and experiment in order to determine the mud layer thickness for maximum wave attenuation in the coast of Suriname.

A.2 Results on reproduction of earlier work

A.2.1 Experiment 1: 1D case Winterwerp 2007.

The first, 1D case where SWAN-Mud is tested is a laboratory experiment that was first conducted by De Wit (1995). A comparison between the results from (Winterwerp, 2007) and the simulations with the latest version of SWAN-Mud is presented in Figure A.1.

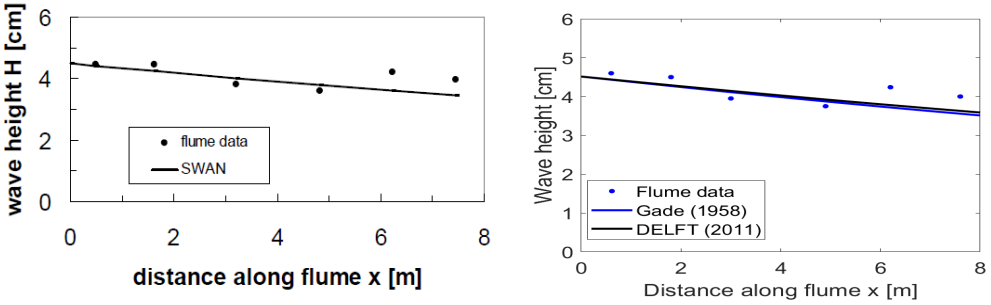

Figure A.1: Measured and computed significant wave height for H_{sig} = 0.045 m, h_w = 0.325 m, h_m = 0.115 m, ρ_w = 1000 kg/m^3, ρ_m = 1300 kg/m^3. Left: Winterwerp (2007). Right: Model outputs from SWAN-Mud: Gade (1958)(blue), Kranenburg (2011) (black) and measurements from laboratory experiment De Wit (1995)

The results from SWAN-Mud are in agreement with the results in (Winterwerp, 2007) where a reduction of the order 20% is observed. In the current experiments, there is 22.18% wave attenuation by the end of the experiment with Gade formulation and 20.51% with DELFT formulation. The RMSE of the wave height between the experiment results from the (schematically estimated) flume data and model outputs is 0.313 m with Gade formulation and 0.2849 m with DELFT formulation.

A.2.2 Experiment 2: Effect of the mudbanks on waves - Guyana case.

The second experiment that takes place in order to compare SWAN-Mud with results from previous studies is a 2D case in Guyana. This experiment was first conducted by Winterwerp (2007), with the initial SWAN-Mud version. Figure A.2a shows the bathymetry and Figure A.2b shows the mud layer thickness that was used in (Winterwerp, 2007).

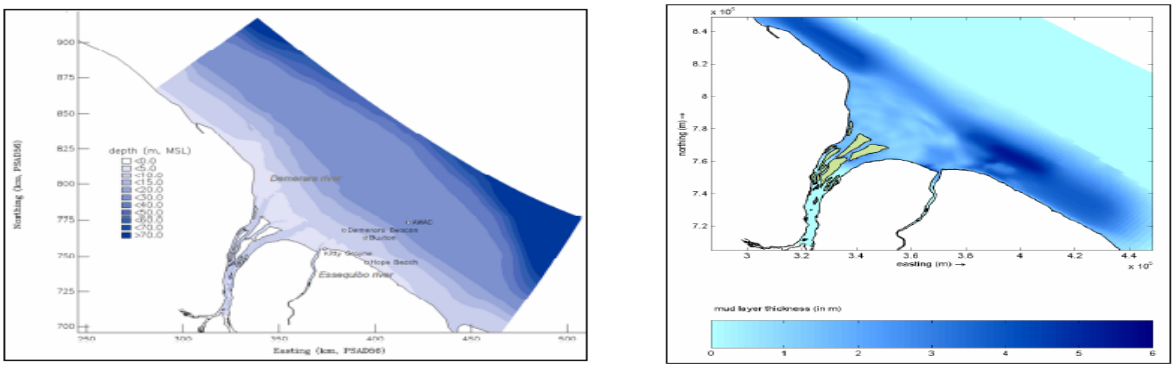

(a) (b)

Figure A.2: Guyana case: (a) Water depth in [m], (b) Mud layer thickness in [m] used in (Winterwerp, 2007).

The case of extreme conditions was studied in Guyana, i.e. wind input of 12.5 m/s and significant wave height of 4 m. In order to repeat the same experiment, an example bathymetry from the JEBCO dataset is used, and the mud layer thickness is designed with the same tools described in Section 2.2.2, i.e. the tools Delft3d-RGFGRID and Delft3d-QUICKIN. Figure A.3 shows the bathymetry and mud layer thickness that were used in order to repeat an experiment similar to the one described in (Winterwerp, 2007). Taking into account the lack of the original data, i.e. the original water depth and mud layer thickness deviations from the outputs in (Winterwerp, 2007) are expected.

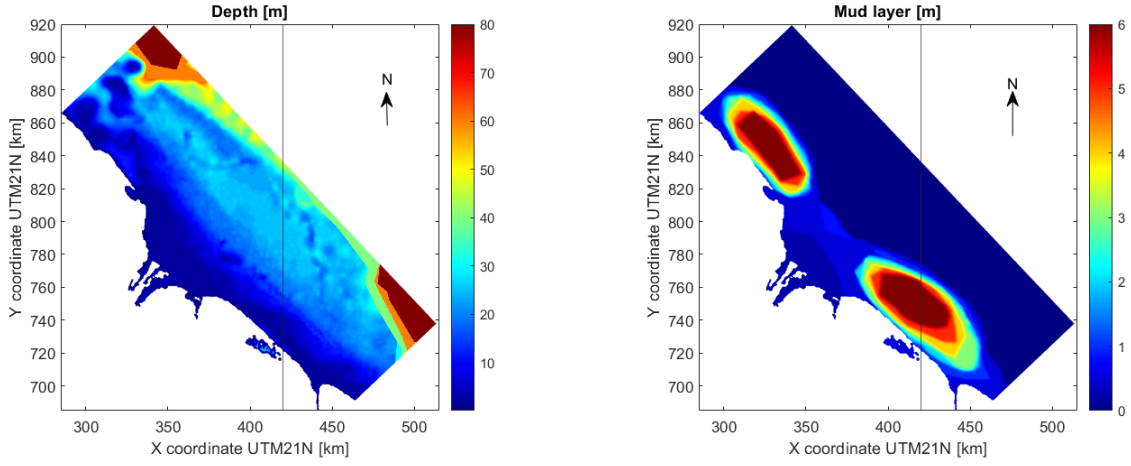

(a) (b)

Figure A.3: Guyana model set up. (a): Water depth [m] (b): Mud layer thickness [m]. The black line indicates the cross-section where significant wave height, wave period and total dissipation are analyzed.

Two cases are compared in (Winterwerp, 2007). One with the mud layer thickness indicated in

Figure A.2b and one without it. The same experiment is conducted for the purposes of this report with SWAN-Mud and the formulations of Gade and DELFT.

The comparison between the case in Guyana from (Winterwerp, 2007) and the one with SWAN-Mud v40.61 is successful in case the DELFT formulation is used. In the left plots of Figure A.4, the significant wave height instantly decreases as soon as waves approach to the mud layer in contrast to the case without mud, where significant wave height decreases only when the water depth is small enough to induce depth-induced wave breaking. The wave period decreases soon after the waves start propagating in the mud layer, while in the case without mud the wave period decreases only very close to the shore. A similar behaviour is observed for the total dissipation. In case of mud, there is an instant peak in wave dissipation, observed exactly at the location where the mud layer starts. No other peaks are obvious as the waves are already attenuated and do not break further closer to the coast. The bottom profile is also very smooth and contributes to this behaviour. In the case without mud, the waves dissipate only very close to the shore, probably due to depth-induced wave breaking.

However, in case of Gade there is a significant difference when the wave period is studied compared to the results from Winterwerp (2007). Although the wave period significantly decreases when the waves arrive at the mud layer, the wave period very close to the shore increases sharply. This is not the case with DELFT parameterization, where wave period is constantly decreasing. The unexpected behaviour that is observed with Gade's parameterization is explained in Wells and Coleman (1981) and also with the use of the wave spectra in similar locations as shown in Figure A.4 . The reason for the shift of wave energy towards lower frequencies when waves approach the coast is

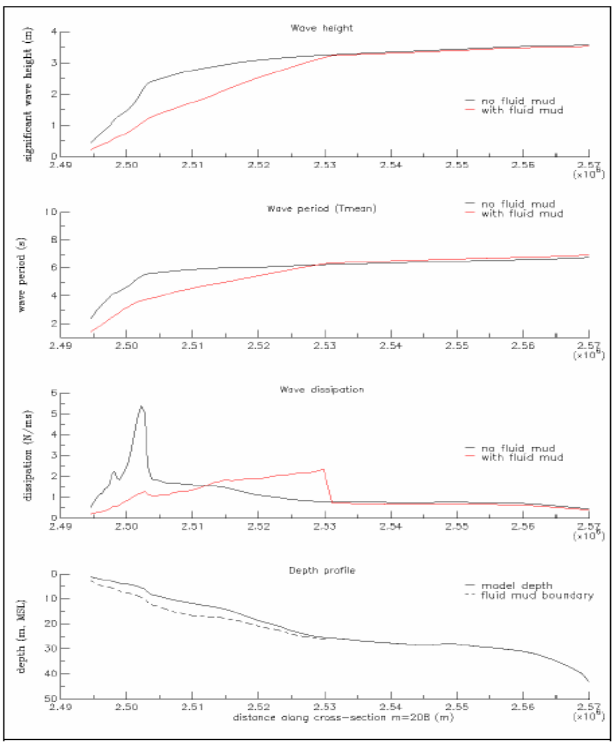

(a) Winterwerp (2007)

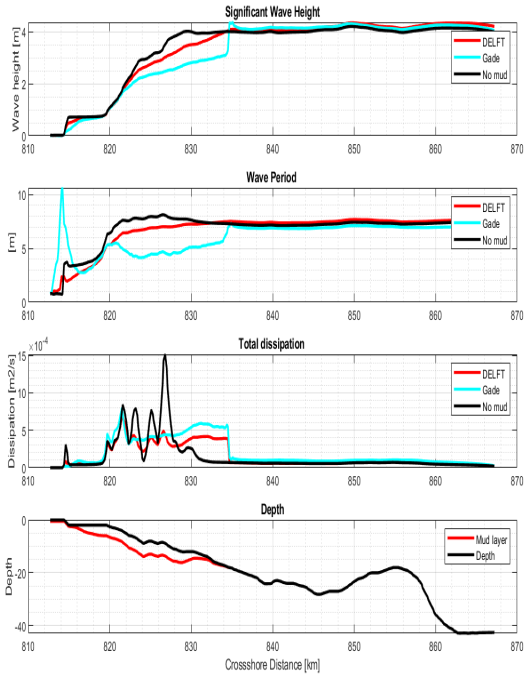

(b) Simulations SWAN-Mud 2020

Figure A.4: From top to bottom: Cross-shore profiles of significant wave height [m], wave period [s], total dissipation[m^2/s], mud layer thickness [m], water depth [m]. Waves propagate from the offshore part (right side) towards the coast (left side). Outputs from SWAN-Mud for the case in Guyana.

the attenuation of waves due to whitecapping which took place offshore (due to the large significant wave heights). As a result, the majority of waves that approach the coast have already dissipated and belong to the low-frequency part of the wave spectrum.

Winterwerp (2007) compares the case where wind and waves force the system in the initial simulations (discussed earlier), with a case where only waves force the system. This comparison takes place in this report as well. The wave spectrum is computed for three different locations with both Gade and DELFT formulation: a location far offshore of the coast, a location at an intermediate water depth and a location very close to the shore. Besides the fact that wave energy is strongly decreased when the waves are propagating towards the coast in both cases, in the cases where the system is forced with wind, there is a pronounced shift in larger frequencies compared to the cases without wind (top plots, Figure A.5). In the offshore location, most energy is accumulated in low frequency waves for both formulations as can be seen in the peaks of 0.1Hz in the same plots. However, energy is decreased in case of Gade formulation compared to DELFT even in the offshore part, with this being more pronounced in the starting point of the mudbanks in both cases, with and without wind (middle plots, Figure A.5). At 0.1 Hz the energy is in the order of 10-20 m^2/s, while in the offshore part it was in the order of 20-30 m^2/s. Closer to the shore there is a clear shift in larger frequencies in the cases with wind for both formulations (bottom plots, Figure A.5). The second peak is found at 0.32 Hz with Delft formulation and at 0.38 Hz with Gade formulation). In case of Gade, waves are shifted to larger frequencies compared to DELFT formulation. As already explained, in this case low frequency waves have been already dissipated and mainly high frequency waves arrive at the shore. A direct comparison of wave energy between the case in Winterwerp (2007) and here doesn't take place, as the set up of the model is much different, and only the pattern of the wave parameters is compared.

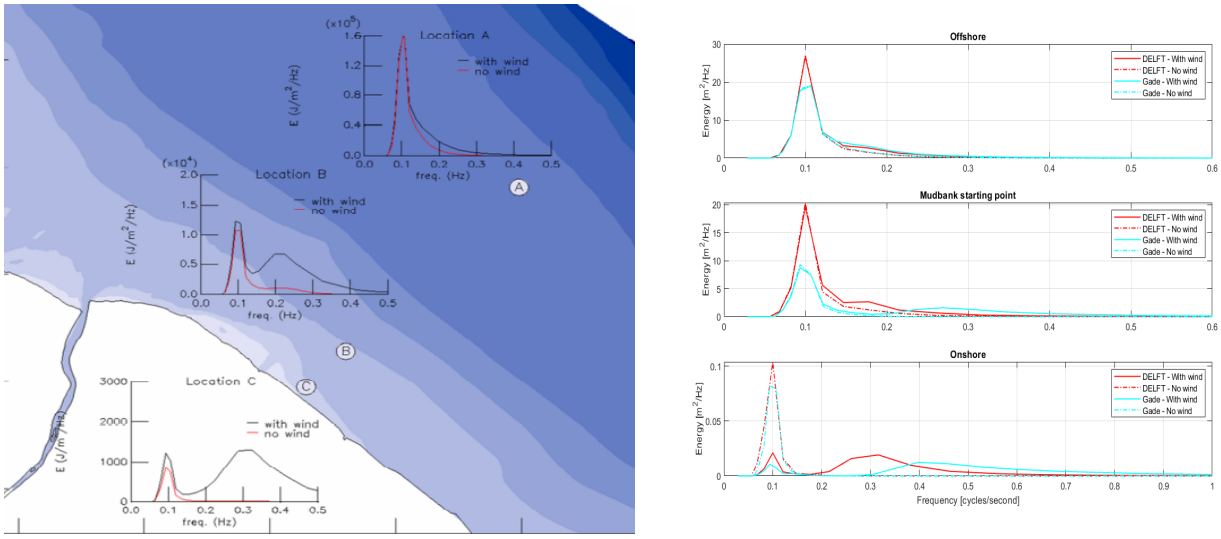

(a) (b)

Figure A.5: (a): Figure 13 (Winterwerp, 2007). Wave spectra computed in three locations, with changing distance from the coast of Guyana. Far offshore of the coast, very close, and in between. (b) Model outputs from SWAN-Mud for three similar locations. The same behaviour is observed in both cases. While waves propagate towards the coast, they lose energy. A shift in larger frequencies shows the transition from swell waves to wind waves.

A.2.3 Experiments 3 and 4: Optimum mud layer thickness for maximum wave attenuation.

As described in methodology Section A.1 different formulations for wave damping that are implemented in SWAN-MUD were tested by Kranenburg (2011). The comparison takes place by computing the mud layer thickness that induces maximum wave attenuation, i.e. for which mud layer thickness k_i is the largest. These computations result in approximately the same (optimum) mud layer thickness with each of these formulations. For the purpose of testing SWAN-mud V40.61 the same experiments were repeated (Experiment 3, Table A.4). However, the results deviate from Kranenburg (2011), and an optimum mud layer thickness is found only in the case of Gade and Ng. In case of DELFT and De Wit formulation k_i is continuously decreasing for increasing mud layer thicknesses. Comparison takes place in Figure A.6.

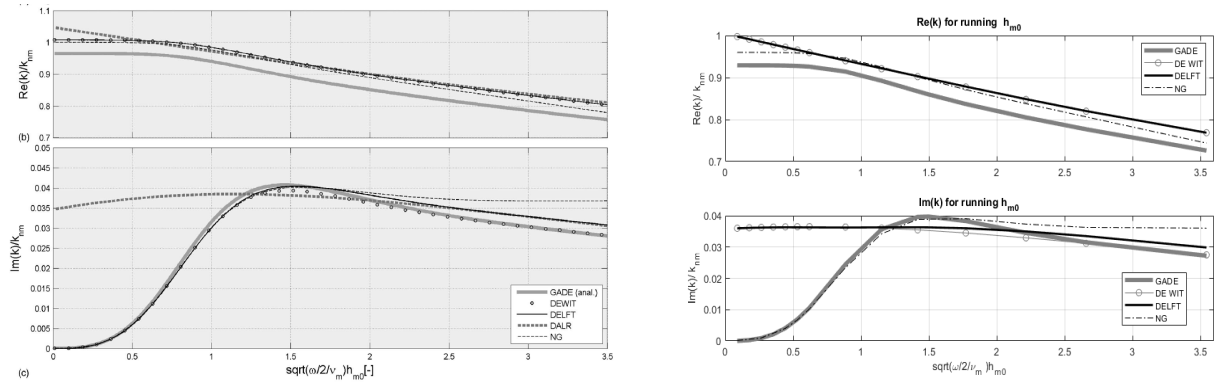

(a) (b)

Figure A.6: (a): Mud layer thickness computation for maximum wave attenuation (figure taken from (Kranenburg, 2011)) (b) Same experiment, simulations with SWAN-Mud v40.61. Model inputs for both cases: H_w = 4 m, T = 8 s, ρ_m = 1750 kg/m^3, ν_m = 0.5 m^2/s. Mud layer thickness (x-axis) is scaled with the boundary layer thickness $\delta_{BL} = \sqrt{\frac{2\nu}{\sigma}}$ and k_i is scaled with the wave number k for situations without (fluid) mud.

The same behaviour is obtained when repeating an experiment conducted by De Wit (1995)(Experiment 4, Table A.4). De Wit performed a similar experiment, computed the mud layer thickness which induces maximum wave attenuation, but for the model he developed in De Wit (1995). Computations with SWAN-Mud v40.61 reveal an optimum mud layer thickness only in case of Gade and Ng formulations, Figure A.7. Although in this case a comparison between the different formulations by De Wit does not take place, his results are used in order to test the validity of SWAN-Mud.

A.2.4 Implications of the results

Regarding the 1D Experiments 1, 3 and 4 all original inputs are available, so an accurate comparison between the original results (De Wit, 1995; Winterwerp, 2007) and the results from SWAN-Mud can take place. Experiment 1 shows good agreement with the results from Winterwerp (2007). Significant wave height is expected to reduce by 20%. Gade formulation results to a reduction of 22.18% and DELFT formulation to a reduction of 20.51%. This is a first indication that Gade's formulation overestimates wave dissipation.

Experiments 3 and 4 aim at reproducing the results from Kranenburg (2011), and more particularly the optimum mud layer thickness for maximum wave attenuation. The results from the current version of SWAN-Mud (v40.61) are not in accordance with the results from the SWAN-Mud version

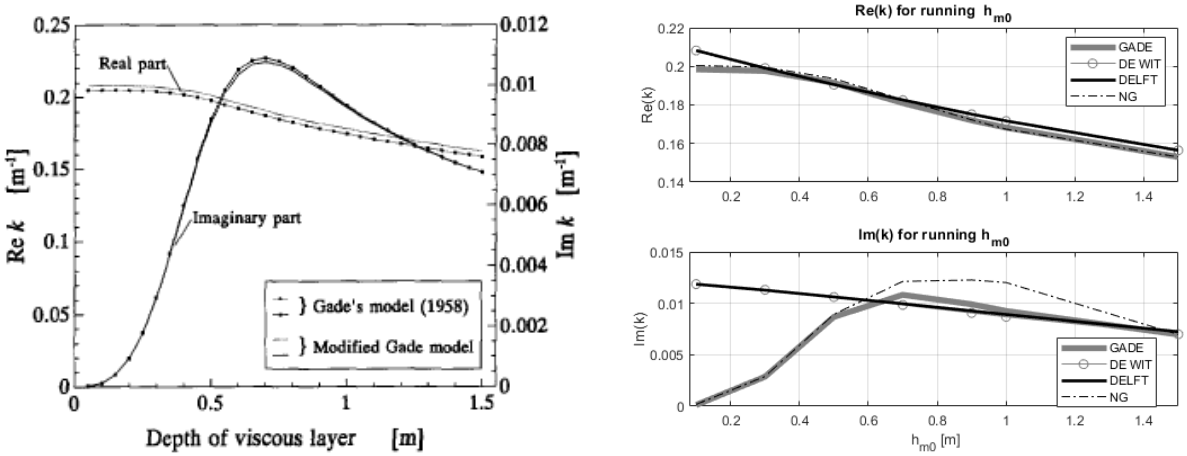

(a) (b)

Figure A.7: (a): Figure 3.4.5 (De Wit, 1995), mud layer thickness computation for maximum wave attenuation. (b) Same experiment, simulations with SWAN-Mud v40.61. Model inputs for both cases: H_w = 1.5 m, T = 8 s, ρ_m = 1500 kg/m^3, ν_m = 0.1 m^2/s. Mud layer thickness (x-axis) is scaled with the boundary layer thickness $\delta_{BL} = \sqrt{\frac{2\nu}{\sigma}}$ and k_i is scaled with the wave number k for situations without (fluid) mud.

that was used in Kranenburg (2011) (Experiment 3). In particular, it is not possible to obtain an optimum mud layer thickness with DELFT and De Wit formulation. In experiments with this formulations, k_i (exponential decay of waves) does not attain a maximum value, but it is decreasing with increasing mud layer thickness (Figures A.6 and A.7). This is only possible with Gade formulation. The same experiment was also done with an other formulation in SWAN-Mud, i.e. with Ng (2000), but it is not analyzed in the chapter with the results. The desired optimum mud layer thickness is also obtained with this formulation. However, 2D experiments fail to give outputs of the standard form, but only NaN values (Not-a-Number values). This is the reason why this formulation is not used throughout this report. The same pattern is observed when trying to obtain an optimum mud layer thickness during Experiment 4. It is not possible to obtain an optimum mud layer thickness with Delft and De Wit parameterizations, but only with Gade and Ng (Ng, 2000). The results of both Experiments 3 and 4 indicate technical issues in the used version of SWAN-Mud with DELFT and De Wit formulations, meaning that the actual formulations that were developed by Kranenburg (2011) and De Wit (1995) are not implemented correctly in the source code of SWAN-Mud.

A second explanation for the difference in the results is that the manual for SWAN-Mud v40.61 contains errors. SWAN-Mud can be used only if a specific formulation is selected (Gade: (Gade, 1958), Dalrymple: (Dalrymple and Liu, 1978), De Wit: (De Wit, 1995), Ng: (Ng, 2000), Guo: Guo (2002), DELFT: Kranenburg (2011)) and there is no default formulation specified by the model. A formulation can be selected by specifying a certain number i.e. 1 corresponds to Gade, 2 corresponds to De Wit, etc. The possible error is that the order of the formulations may have been different from what is stated in the manual for SWAN-Mud v40.61, as will be elaborated in the following paragraphs. This possibility was tested with the following experiment.

The process of performing experiments in shallow and deep waters, taking into account the strong shallow water limitation in case of Gade (1958), $kH \ll 1$ (end of section 2.1.1.3, can possibly give a better picture about the consistency between the formulations in the manual and the formulations in the model. Figure 2 from Kranenburg (2011) compares the latest (by then) SWAN-Mud version, with the one that was used by Winterwerp (2007) (including De Wit (1995) formulation) and with a

simple analytical solution, which is not of interest now. What is tested, is the significant wave height when waves propagate towards a mud layer. It is expected that the two models (DELFT and De Wit formulations) will show the same pattern in case of shallow water but a different one in case of deep waters. This expectation is confirmed in Kranenburg (2011). The same experiment is repeated with SWAN-Mud v40.61 in this report. Due to the uncertainties revealed in the previous experiments (1D experiments 3 and 4), simulations with all the available formulations in SWAN-Mud take place. The results are available in Figure A.8 .

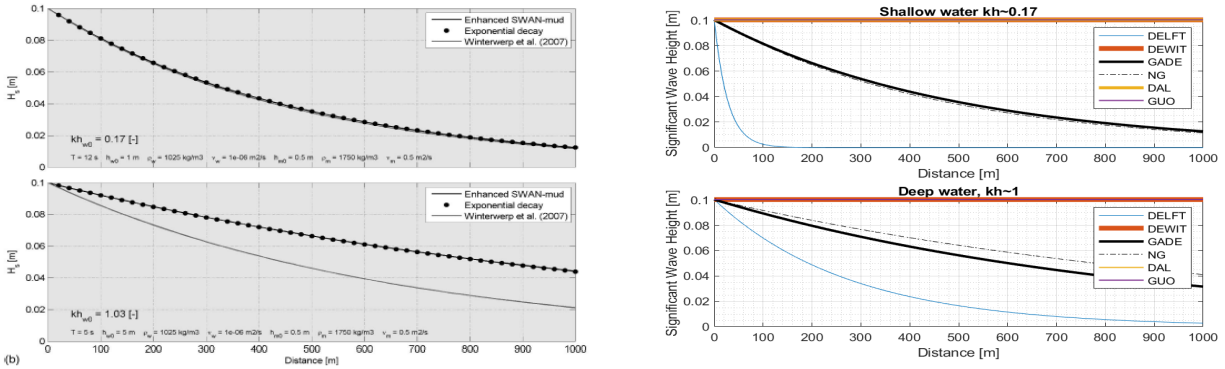

(a) (b)

Figure A.8: (a): Figure 2 from Kranenburg (2011), significant wave height in the case of waves propagating over a constant mud layer(h_m = 0.5 m in shallow waters ($kH_w \approx 0.17$). Model inputs: H_w = 1 m, T = 12 s, h_m = 0.5 m, ρ_m = 1500 kg/m^3, ν_m = 0.1 m^2/s. and in deep waters ($kH_w \approx 1.03$). Model inputs: H_w = 5 m, T = 5 s, h_m = 0.5 m, ρ_m = 1500 kg/m^3, ν_m = 0.1 m^2/s. (b) Same experiment, simulations with SWAN-Mud v40.61.

In the current study, the significant wave height decreases almost instantly in case of DELFT (enhanced SWAN-Mud) for the shallow water case, i.e. in the first 100 m while wave height is expected to be 0.01 m in the end of the domain in Kranenburg (2011), Figure 2. In case of deep water, the significant wave height for the same formulation, dissipates more than expected, i.e. H_{sig} = 0.01 m while expected H_{sig} = 0.2 m in the end of the computation. Gade and Ng, in case of shallow water, show exactly the expected behaviour from Delft formulation (enhanced SWAN-Mud), while for deep water, Gade again shows the expected behaviour in the case of DELFT formulation. Consequently, the dispersion relation that should contain Gade's formulation, may actually represent one of the other formulations. The results shown here suggest that it may have been the DELFT formulation, although that should be confirmed. This is only a possibility, and the way to accurately examine if there are inconsistencies between the manual and the model, is to compile the source code of SWAN-Mud and test the different formulations.

Experiment 2 (2D case in Guyana) confirms the findings of Experiment 1 (1D laboratory case), i.e. that the formulation of Gade overestimates wave dissipation compared to DELFT formulation. The cross-section in Figure A.4 indicates the steeper decrease of significant wave height and the steeper increase of total dissipation as soon as the waves meet the mud layer. Overestimation of wave attenuation probably results in dissipation of all high-frequency waves. As a result, when the waves arrive at the coast the spectra is dominated by low-frequency waves (large wave period waves). This is also the finding of the observations from Wells and Coleman (1981). However, findings from Winterwerp (2007) are in better agreement with the results from DELFT formulation. Instant dissipation of waves occurs as soon as they arrive at the mud layer, however not strong enough in order to dissipate so efficiently low-frequency waves. According to the results in the same figure, there is evidence that Gade formulation overestimates dissipation also due to white-capping. This

is confirmed according to the wave spectra, where the reduced wave energy is observed with Gade formulation in the offshore location, compared to the results from DELFT formulation. However, both formulations indicate a shift of the wave energy to larger frequencies very close to the shore in the cases with wind, compared to the cases without wind.

Bibliography

Edward Anthony. Fluvial sediment supply, mud banks, cheniers and the morphodynamics of the coast of south america between the amazon and orinoco river mouths. *Geological Society London Special Publications*, 2013. doi: 10.1144/SP388.8.

Edward Anthony and Nicolas Gratiot. Coastal engineering and large-scale mangrove destruction in guyana, south america: Averting an environmental catastrophe in the making. *Ecological Engineering*, 2012. doi: 10.1016/j.ecoleng.2012.07.005.

Edward Anthony, Franck Dolique, Antoine Gardel, Nicolas Gratiot, Christophe Proisy, and Laurent Polidori. Nearshore intertidal topography and topographic-forcing mechanisms of an amazon-derived mud bank in french guiana. *Continental Shelf Research*, 28(6):813 – 822, 2008. ISSN 0278-4343. doi: https://doi.org/10.1016/j.csr.2008.01.003. URL http://www.sciencedirect.com/science/article/pii/S0278434308000083.

P.G.E.F. Augustinus. The changing shoreline of suriname (south america). 1978. URL https://dspace.library.uu.nl/handle/1874/263140.

Pieter G.E.F. Augustinus. Actual development of the chenier coast of suriname (south america). *Sedimentary Geology*, 1980. doi: https://doi.org/10.1016/0037-0738(80)90007-X.

Pieter G.E.F Augustinus. The influence of the trade winds on the coastal development of the guianas at various scale levels: a synthesis. *Marine Geology*, 208(2):145 – 151, 2004. ISSN 0025-3227. doi: https://doi.org/10.1016/j.margeo.2004.04.007. URL http://www.sciencedirect.com/science/article/pii/S0025322704001045.

Siadatmousavi Beyramzade. Implementation of viscoelastic mud-induced energy attenuation in the third-generation wave model, swan. *Ocean Dynamics*, 2018. doi: 10.1007/s10236-017-1118-4. URL https://doi.org/10.1007/s10236-017-1118-4.

N. Booij. A third-generation wave model for coastal regions: 1. model description and validation. *Journal of Geophysical Research: Oceans*, 1999. doi: 10.1029/98JC02622.

Encyclopaedia Britannica. Stewart island, 2007. URL https://www.britannica.com/science/island.

Robert Dalrymple and Philip Liu. Waves over soft muds: A two-layer fluid model. *Journal of Physical Oceanography*, 8:1121–1131, 11 1978. doi: 10.1175/1520-0485(1978)008⟨1121:WOSMAT⟩2.0.CO;2.

Davis and Fitzgerald. Beaches and coasts richard a. davis, duncan m. fitzgerald. *Estuarine Coastal and Shelf Science - ESTUAR COAST SHELF SCI*, 2005. doi: 10.1016/j.ecss.2004.11.006.

De Wit. Liquefaction of cohesive sediments caused by waves. 1995.

J.M Froidefond, M Pujos, and X Andre. Migration of mud banks and changing coastline in french guiana. *Marine Geology*, 84(1):19 – 30, 1988. ISSN 0025-3227. doi: https://doi.org/10.1016/0025-3227(88)90122-3. URL http://www.sciencedirect.com/science/article/pii/0025322788901223.

Gade. Effects of a non-rigid, impermeable bottom on plane surface waves in shallow water. *Journal of Marine Research, 16(2), 61–82.*, 1958.

GEBCO. *Computers Geosciences*. URL https://www.gebco.net/data_and_products/gridded_bathymetry_data/.

W.R. Geyer, P.S. Hill, and G.C. Kineke. The transport, transformation and dispersal of sediment by buoyant coastal flows. *Continental Shelf Research*, 2004. doi: https://doi.org/10.1016/j.csr.2004.02.006.

Junke Guo. Simple and explicit solution of wave dispersion equation. *Coastal Engineering*, 45:71–74, 04 2002. doi: 10.1016/S0378-3839(02)00039-X.

Terry R. Healy. *Muddy Coasts*, pages 674–677. Springer Netherlands, Dordrecht, 2005. ISBN 978-1-4020-3880-8. doi: 10.1007/1-4020-3880-1_220. URL https://doi.org/10.1007/1-4020-3880-1_220.

L. Holthuijsen. Waves in oceanic and coastal waters. *Cambridge University Press.*, 2007. doi: 10.1017/CBO9780511618536.

Boris Kagan and Ekaterina Sofina. Surface and internal semidiurnal tides and tidally induced diapycnal diffusion in the barents sea: A numerical study. *Continental Shelf Research*, 91, 12 2014. doi: 10.1016/j.csr.2014.09.010.

Wouter Kranenburg. Modelling wave damping by fluid mud. *MSc. Thesis*, 2008.

Wouter Kranenburg. Swan-mud: engineering model for mud-induced wave damping. *Journal of hydraulic engineering, 137(9), 959 - 975. American Society of Civil Engineers. ISSN 0733-9429.*, 2011. doi: 10.1061/(ASCE)HY.1943-7900.0000370.

Philip Liu and I-Chi Chan. A note on the effects of a thin visco-elastic mud layer on small amplitude water-wave propagation. *Coastal Engineering - COAST ENG*, 54:233–247, 03 2007. doi: 10.1016/j.coastaleng.2006.08.015.

Hugh Macpherson. The attenuation of water waves over a non-rigid bed. *Journal of Fluid Mechanics*, 97(4):721–742, 1980. doi: 10.1017/S0022112080002777.

manual Delft3D-FLOW. URL https://oss.deltares.nl/documents/183920/185723/Delft3D-FLOW_User_Manual.pdf.

Robert Morton, Tara Miller, and L. Moore. National assessment of shoreline change: Part 1 historical shoreline changes and associated coastal land loss along the u.s. gulf of mexico. 01 2004.

Nedeco. Surinam transportation study: Report on hydraulic investigation. 1968.

Chiu-On Ng. Water waves over a muddy bed: A two-layer stokes' boundary layer model. *Coastal Engineering*, 40:221–242, 06 2000. doi: 10.1016/S0378-3839(00)00012-0.

Erftemeijer Paul. Iczm plan suriname-mangrove report. 2009. doi: https://www.academia.edu/2169366/ICZM_Plan_Suriname_Mangrove_Report.

Rich Pawlowicz, Bob Beardsley, and Steve Lentz. Classical tidal harmonic analysis including error estimates in matlab using t_tide. *Computers Geosciences*, 28(8):929 – 937, 2002. ISSN 0098-3004. doi: https://doi.org/10.1016/S0098-3004(02)00013-4. URL http://www.sciencedirect.com/science/article/pii/S0098300402000134.

David Pugh and Philip Woodworth. *Sea-Level Science: Understanding Tides, Surges, Tsunamis and Mean Sea-Level Changes*. Cambridge University Press, 2014. doi: 10.1017/CBO9781139235778.

Andrew D. Short. *Sandy Coasts*, pages 821–825. Springer Netherlands, Dordrecht, 2005. ISBN 978-1-4020-3880-8. doi: 10.1007/1-4020-3880-1_267. URL https://doi.org/10.1007/1-4020-3880-1_267.

M.C. Simpson, Daniel Scott, Mark New, R. Sim, D. Smith, M. Harrison, C. Mark Eakin, R. Warrick, Alan Strong, P. Kouwenhoven, Stephan Harrison, M. Wilson, G.C. Nelson, Simon Donner, Robert Kay, D.K. Gledhill, Gang Liu, Jessica Morgan, Joan Kleypas, and H. Stager. An overview of modeling climate change impacts in the caribbean region with contribution from the pacific islands. 01 2009. URL https://coralreefwatch.noaa.gov/satellite/publications/UNDP_Final_Report.pdf.

Erik Toorman, Edward Anthony, Pieter Augustinus, Antoine Gardel, nicolas gratiot, Oudho Homenauth, Nicolas Huybrechts, Jaak Monbaliu, Kene Moseley, and Sieuwnath Naipal. Interaction of mangroves, coastal hydrodynamics, and morphodynamics along the coastal fringes of the guianas. pages 429–473, 04 2018. doi: 10.1007/978-3-319-73016-5_20.

John T. Wells and James M. Coleman. Physical processes and fine-grained sediment dynamics, coast of surinam, south america. *Journal of Sedimentary Research*, 1981. doi: 10.1306/212F7E1E-2B24-11D7-8648000102C1865D.

Winterwerp. Modelling of wave damping at guyana mud coast. *Coastal Engineering*, 2007. ISSN 0378-3839. doi: https://doi.org/10.1016/j.coastaleng.2006.08.012.